Multiscale simulation of flow and heat transport in fractured geothermal reservoirs

Tor Harald Sandve

Dissertation for the degree of Philosophiae Doctor (PhD)

Department of Mathematics
University of Bergen

December 2012

Preface

The energy demand in the world has increased tremendously during the last centuries. A growing population combined with increasing welfare throughout the world is the driving force behind the rising energy demand. Moreover, as the vast population living in the developing countries in Asia, South-America and Africa takes part in a more westernized and thus energy consuming life, the demand will continue to grow far into the future. Fossil fuels are the main supplier of energy in the world today, and according to the International Energy Agency (IEA) it will continue to be the most important source of energy for a long time. It is however likely that the massive usage of fossil fuel threatens the climate on our planet. A part from the local pollution coming from usage of fossil fuels as smog and NO_x, fossil fuels emit CO_2 into the atmosphere. The challenge is therefore twofold: providing the world with energy, but in a sustainable way that do not threaten our environment and our future.

High expectations have been placed upon the renewable energies, especially the unconventional sources as solar, wind and geothermal energy. Can they provide the energy the world needs? According to IEA the utilization of these unconventional sources provided less than 1% of the world's total energy supply in 2009. For these energy sources to provide more than a marginal part of the future energy supply, a massive and combined effort from policymakers, R/D and the industry is necessary.

Geothermal energy is attractive as an energy source mainly because of its enormous potential and ability to provide base-load power. This is in contrast to wind and solar energy that are dependent on the weather conditions and time of day and year. Traditionally, it has been thought that geothermal energy is restricted to specific countries with favorable conditions, such as Iceland and the Philippines, but resent improvements in reservoir technology, drilling and management, have opened up new possibilities for geothermal energy to provide energy anywhere in the world. In 2011 IPCC identified the need for improved numerical simulation models as an important step towards developing geothermal resources. My hope is that this thesis can contribute towards this goal.

Acknowledgements

First, I would like to thank colleagues at the University of Bergen. This dissertation had not been what it is without the inspiration and the guidance of many and foremost among them, my main supervisor Inga Berre. Her enthusiasm for science and faith in me has affected me greatly. She has together with my co-supervisor Jan Martin Nordbotten given me indispensable help and advice, as they have always been more than willing to share their expert knowledge with me. I have also greatly benefited from collaboration with colleagues, and especially Eirik Keilegavlen. The many discussions we have had, both scientific and less scientific have greatly enriched my time as a Ph.D. candidate and given me valuable new insights. The financial support given by the Research Council of Norway (#190761/S60) is also highly appreciated.

Last but not least, I would like to thank my family. My one year old son Johannes, for helping me forget my work when I am home and my wife Ingelin for always being supportive and caring.

Introduction

Geothermal energy is the thermal energy stored in the Earth's crust. The average heat flux that leaves the surface of the earth is 60 mW/m^2 of which around 50-80% is generated by radioactivity within the earth. The geothermal energy source is utilized by extracting the energy stored in the crust. This will temporarily and locally cool down the crust, but with time, heat from the surroundings will regenerate the temperature in the area. It is common to divide the geothermal resources into three categories; shallow and low temperature resources used for direct heating, hydrothermal resources and enhanced geothermal systems (EGS).

The low temperature systems account for two thirds of the produced geothermal energy [36]. In geothermal active regions, hot water welling up from the surface is used directly both for space heating and in public bathhouses and swimming pools, while geothermal heat pumps (ground source heat pumps) are used in less geological active regions. Both rock and water have larger heat capacity than air and higher efficiency is thus obtained for the geothermal heat pumps compared to standard air-to-air pumps. In addition, heat extracted during the winter can be returned during summer time, creating sustainable systems.

The hydrothermal systems are situated in geological active regions known as "the ring of fire", that includes countries such as Iceland, the USA, Mexico, Philippines, Japan, Italy and Indonesia. In these regions all the necessary ingredients to establish a geothermal system can be found. These include high temperatures close to the surface due to volcanic activity, fluid to transport the heat, and a reservoir of porous rocks with fractures where the fluid can flow. The economy of the geothermal systems depends largely on the flow rates and the temperatures in the production wells. To enhance the production, multiple of both production and injection wells are drilled, and water is injected to support the pressure in the reservoir. In 2010 a total of 66TWh/year of electric energy was produced from hydrothermal systems [48].

Combining the supply of energy from all geothermal sources still only accounts for 0,1% of the total energy supply in the world [10]. If geothermal energy is to play a role in future energy portfolio, it has to expand from being restricted to geothermal active regions, where hydrothermal reservoirs exist naturally, to become a global resource. Recent improvements in drilling technology and reservoir engineering have fortunately opened up possibilities to utilize the geothermal energy in larger regions. According to the recent IPCC report, so-called Enhanced Geothermal Systems (EGS) have potential to provide a significant part of the world's energy supply [36].

In EGS one or more of the conditions required to have a natural hydrothermal system are lacking. The necessary conditions are instead created artificially. High temperatures are reached by drilling deep wells. With an average thermal gradient at 25 °C/km, a reservoir at 5 km depth will have a temperature over 125 °C, a temperature

sufficient to operate a power plant. If the reservoir is dry, water is injected to transport the energy from the reservoir to the production wells. After the hot fluid is used, it can be re-injected in order to create a circulation loop. The most challenging part of an EGS is to create the reservoir itself. The reservoir is created by establishing a connected pathway between the injecting wells and the producing wells. The most common technique is hydraulic fracturing, where fluid is pumped into wells at sufficiently high pressure to open fracture networks [36]. Fractures will then open in the least stress direction and develop normal to the this. In most part of the world, except Australia, the least stress direction is horizontal and thus nearly vertical fractures are created. Other fracturing techniques that are used are thermal stimulation and acid stimulation [36]. For the reservoir to be an efficient heat exchanger, the contact surface between the fluid and the rock must be maximized. If most of the fluid runs in large fractures directly connecting the wells, the fluid temperature will rapidly decrease as the heat conduction in the rock is not sufficient to replace the extracted heat. To avoid short circuiting and rapid temperature drops in the wells, care must be taken when the reservoir is created.

A key to successful utilization of geothermal energy is to manage the energy resource in a sustainable way. In early geothermal literature, geothermal energy was characterized as a mining process since an over exploitation of the resource leads to rapid depletion locally. Rybach among others, however stress the fact that sustainable production can be achieved by using moderate production rates that take into account the local resource characteristics (field size, natural recharge rate etc.) [93]. To quantify suistanable production rates numerical simulations of mass and heat transfer are needed. Numerical simulations are a powerful tool to quantify and deepen the understanding of the relevant processes in a geothermal system. It can guide the engineers in the design of the reservoir, in finding optimal well locations and determining optimal well management. It can also be used to quantify the potential of the geothermal resources present at a location, and thus *a priori* provide valuable information on whether the project is feasible from an economical perspective, or not.

Simulation of geothermal systems are challenging as it involves highly complex and coupled non-linear processes on a multiple of time and length scales. Five main remaining challenges are identified in [32]. The three first challenges are related to developing realistic, fully coupled Thermal-Hydro-Mechanical-Chemical (THMC) models that represent all the relevant processes involved during borehole-stimulation and heat extraction. This includes the difficult problem of simulating rock failure, the growth of discrete fractures and the influence of precipitation and dissolution of chemical species on the reservoir. The fourth challenge is related to simulation of large-scale high-resolution models involving discrete fractures and fracture networks, and the associated challenges related to the large span of temporal and spatial scales involved. The fifth challenge is identified as developing improved thermodynamic data and constitutive relations based on laboratory experiments.

The work in this thesis focuses on the fourth challenge related to fractures. Discontinuities in geological formations or rocks are formed as a direct result of applied stress. Geologists distinguish these discontinuities based on their origin as fault, joint, etc..., but from a hydrological perspective it is practical to term all these discontinuities for fractures regardless of their origin or characteristics. Individual fractures can be approximated locally by two-dimensional planes, as one of its lateral extensions, which

is termed aperture, is much smaller than the other two. In general the surfaces of the fractures may not be planar and the void space between the surfaces may be filled with materials. Individual fractures are often connected to other fractures forming complex networks of fractures. Moreover, the host rock between the fractures may itself have holes and pores where fluid can flow and is therefore considered a porous medium. The size of the pores is typically of order of magnitudes smaller than the fracture apertures, meaning that flow in fractures and fracture networks controls the overall flow behavior at the large scale. An appropriate modeling of flow in fractured porous media is therefore crucial for accurate flow predictions as most geothermal reservoirs are fractured [17].

Mechanical and chemical effects are not considered herein. It is however important to keep in mind that the ultimate goal is numerical models that incorporate all the relevant physics, while efficiently giving accurate enough predictions. Recent progress on THMC models for geothermal systems are reported for instance by [26, 33, 54, 86, 103–105, 110, 114, 115]. The coupling of rock mechanics and chemistry to the developed methods for fractures are further discussed in Chapter 4.

The numerical methods and models for flow and transport in fractured porous media presented in this thesis are also highly applicable to other subsurface flow problems. Many oil and gas reservoirs lie in naturally fractured reservoirs [80], and accurate modeling tools are important to enhance the oil and gas recovery. Lately the utilization of shale gas has increased dramatically. To access the shale gas the permeability is increased by hydraulic fracturing similar to what is done in EGS. Also in the context of CO_2 storage and waste disposal, fractures are important. Fractures can for instance be potential leakage points for the CO_2 or the contaminants and increase the area of influence as they provide high-permeable pathways through the reservoir. The author does believe that the contributions of this thesis go beyond its application in geothermal energy, and are relevant for a far broader audience.

The main contributions of this thesis are:

1. **A consistent and robust discretization of flow in fractured reservoirs.** More precisely; an existing numerical method for flow in fractured reservoirs is extended to tackle anisotropic permeabilities on unstructured grids. This extension is important as an unstructured grid is inevitable when complex fracture networks are represented in the grid. The multiscale nature of the fractures motivates using so-called hierarchical approaches where the *small-scale fractures* (as defiend in Chapter 1.1) are represented as upscaled anisotropic permeabilities, while the *large-scale fractures* (as defiend in Chapter 1.1) are model explicitly. The extended method handles both the anisotropy coming from the *small-scale fractures* and the unstructured grid coming from the *large-scale fractures* and is thus highly suitable for such hierarchical approaches.

2. **An efficient linear solver to tackle the high-resolution models stemming from representing individual fractures explicitly.** To construct an efficient linear solver for the high-resolution model two measures are taken. First, the natural scale hierarchy present in fractured reservoirs is exploited to gain efficiency in the solver. Secondly, an inexact approach is used to trade accuracy for efficiency within the framework of an iterative solver. More precisely, the iterative procedure can be stopped whenever the desired accuracy is obtained and still give

conservative fluxes. Taken into account the large uncertainty in the position and geometry of individual fractures such an inexact approach seems reasonable.

3. **A flexible upscaling approach for the heat transport equation, where the fine-scale description is utilized to obtain models tailored for fractured reservoirs.** The flexibility of the upscaling approach allows for the construction of models where the *small-scale fractures* and the porous media is represented in dual-continuum or multiple interacting continuum (MINC) type models and the *large-scale fractures* are represented explicitly. Moreover, as the fine-scale description is used in the upscaling, no heuristic terms are needed to model the interaction between the continua, which is a large advantage with this approach compared to standard dual continuum models.

Outline

This thesis is organized in three parts. The first part includes background theory for the included papers found in Part 2, while Part 3 includes additional papers not regarded as part of the thesis. The background theory in Part 1 is structured as follows: The first chapter includes discussions on modeling concepts for field scale simulations of fractured porous media including both traditional single-scale modeling concepts as well as multiscale concepts. Emphasis is put on linking the relevant temporal and spatial scales to the different modeling concepts. In the second chapter mathematical models for heat and mass transport in porous media are presented briefly, while the third chapter includes theory on numerical models and discretization methods for fractured porous media. In the three first chapters the whole process of going from a description of the physical processes in nature to a numerical model is addressed. The fourth and last chapter includes a summary of the results found in the included papers with comments as well as recommendations for further work.

The five included papers in Part 2 of this thesis are:

Paper A: Sandve, T.H., Berre, I. and Nordbotten, J.M. "An integrated fracture and continuum model for simulating heat and mass transfer in geothermal systems" in proceedings of the 2010 International Groundwater Symposium (IAHR) in Valencia.

Paper B: Sandve, T.H., Berre, I. and Nordbotten, J.M (2012). "An efficient multipoint flux approximation method for Discrete Fracture-Matrix simulations" published in Journal of Computational Physics. 231(9): 3784-3800.

Paper C: Sandve, T.H., Keilegavlen, E. and Nordbotten. "Mass Conservative domain decomposition for fractured porous media" in proceedings of the 2012 XIX International Conference on Water Resources (CMWR 2012) in University of Illinois at Urbana-Champaign.

Paper D: Sandve, T.H., Keilegavlen, E. and Nordbotten, J.M. "Inexact linear solvers for flow in multiscale fractures ", submitted to Water Resources Research, September 2012.

Paper E: Sandve, T.H., Berre, I., Keilegavlen, E. and Nordbotten, J.M. "Multiscale simulation of flow and heat transport in fractured geothermal reservoirs: inexact solvers and improved transport upscaling" in proceedings for the 2013 Stanford Geothermal Workshop.

For completeness, the following coauthored papers are included in the last part. These are not considered the main part of the thesis:

Paper F: Rotevatn, A., Sandve, T.H., Keilegavlen, E., Kolyukhin, D. and Fossen, H. "Deformation bands and their impact on fluid flow in sandstone aquifers: the role of natural thickness variations" submitted to Geofluids, November 2012.

Paper G: Tambue, A., Berre, I., Nordbotten, J.M. and Sandve, T.H. "Exponential Euler time integrator for simulation of geothermal processes in heterogeneous porous

media" in proceedings of the 2012 Stanford Geothermal Workshop.

Contents

Part I

Background

Chapter 1

Conceptual models for fractured porous media

all models are wrong,
but some are useful
George E. P. Box

A conceptual model aims to describe the physical processes relevant for a given purpose at the scale of interest. When designing conceptual models great care must be taken, as the discrepancy between the conceptual representation of the nature and the nature itself cannot easily be assessed. The conceptual modeling influences the mathematical and the numerical modeling, and must therefore be discussed in light of the total modeling process. For instance, the numerical methods presented in Paper A and B for anisotropic permeabilities and the multiscale method presented in Paper C, D and E to tackle high-resolution models are designed to tackle different conceptual representation of *small-scale fractures*. In Paper A and B, *small-scale fractures* are represented as anisotropic permeabilities, while in Paper C, D and E, the *small-scale fractures* are explicitly represented in a multiscale numerical model. In the latter approach the approximations are thus moved from the conceptualization to the numerical modeling. An advantage of the latter approach is that part of the modeling error can be assessed and thus controlled, as more approximations are done within the numerical model instead of in the conceptualization.

To design conceptual models an understanding of how spatial and temporal scales are linked to the relevant physical processes is vital. We therefore start this chapter with a discussion of the relevant spatial and temporal scales involved. Different modeling concepts for field-scale simulation of fractured porous media are then presented based on this discussion.

1.1 Spatial scales

The relevant spatial scales for geothermal simulations are shown in Figure 1.1. The lengths span from kilometer long faults, to pores the size of a few microns. Based on the range of these data we chose to identify four different scales: *mega*, *macro*, *meso* and *micro* (from largest to smallest). Pores and fracture widths belong at the *micro-scale*, together with other features smaller than a few centimeters. Averaged parameters and equations are used to describe the *micro-scale*, as resolving *micro-scale* features in a reservoir scale model are not feasible from a computational perspective,

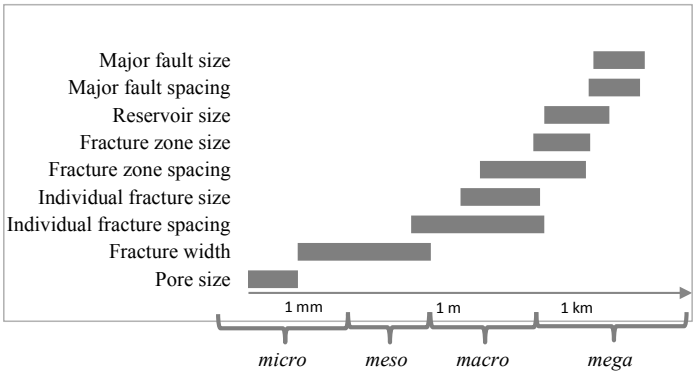

Figure 1.1: Spatial scales

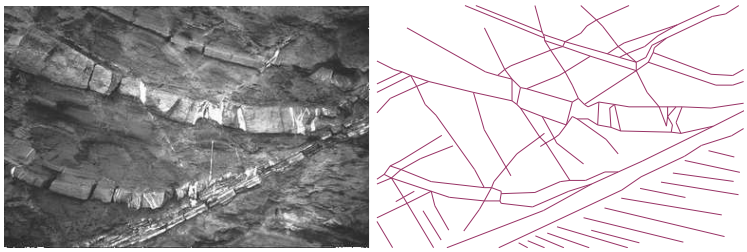

Figure 1.2: A picture of a meter-scale outcrop with conceptual interpretation of layers and fractures (From [43]).

and detailed descriptions of the *micro-scale* are seldom available. Structures between a few centimeters to a meter belong to the *meso-scale*, implying that most individual fractures are resolved at this scale. An example of a *meso-scale* conceptual model of an outcrop with layers and fractures is shown in Figure 1.2. The mathematical equations presented in the next chapter will be defined on the *meso-scale*. On the *macro-scale* only the largest fractures are resolved individually. The resolved fractures are termed *large-scale fractures* to distinguish them from the *small-scale fractures* that are not resolved on the *macro-scale*. The size of the *macro-scale* is typically on the order of tenths of meters. Faults, fracture-zones and long individual fractures are thus considered *large-scale fractures*. Finally, the term *mega-scale* is used for features larger than around 100 m, which includes the size of the reservoir itself and the size of large faults.

1.2 Temporal scales

From a modeling perspective, the time it takes to establish equilibriums is important. For our purpose whether thermal equilibrium is established on the length scales estab-

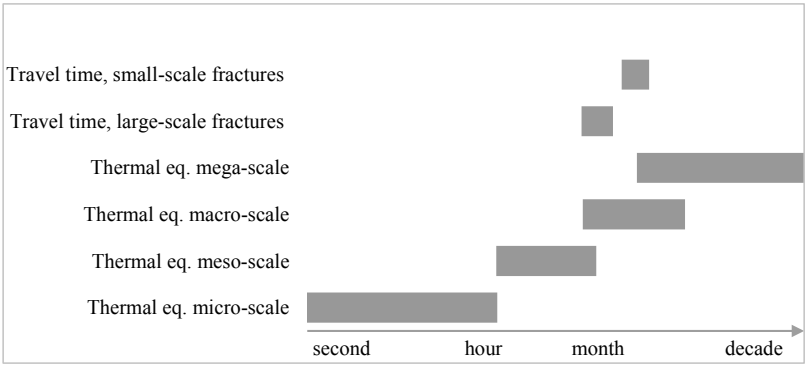

Figure 1.3: Temporal scales

lished in the previous section is of particular interest, as it determines which kind of conceptual models that can be used. Estimates of thermal equilibrium times are shown in Figure 1.3. These estimates are calculated with an order of magnitude analyses, with standard values of the physical parameters [55]. In addition, typical travel times for fluid between the injector and the producer in the EGS site at Soultz are shown as a reference [89]. Thermal equilibrium is obtained in relatively short time on the *micro-scale*. Thermal equilibrium can thus be assumed for most processes occurring at this scale. The conditions for local thermal equilibrium fail in cases where; significant heat generation occur in any of the phases, the temperature at the bounding surface changes rapidly in time, or there is a significant difference in the heat capacities and thermal conductivities of the fluid and solid [55]. In a geothermal setting this may happen in the vicinity of wells, magma chambers or large fractures. On the *meso-scale* the typical equilibrium time is in the order of hours, while it may take months before the temperature is at equilibrium on the *macro-scale*. The time-scale for which equilibrium is obtained at the *meso-* and *macro-scale* is too large to ignore and must be accounted for in the models. The values for the *mega-scale* equilibrium can be seen as rough estimates on the regeneration time for geothermal reservoirs. In some cases the regeneration time may be in the order of the production time itself and continuous production is possible. This may happen in hydrothermal reservoirs where there is a relatively large background flow that supplies heat to the reservoir from its surroundings. For EGS, a realistic time-scale for when the temperature is back to pre-production values ranges from 30-50 years [36] .

1.3 Macro-scale models

The scales on which numerical simulations can be done are restricted by the available computational resources. Even with the help of a tremendous growth in computational power, *mega-scale* simulation models where all *micro-scale* features are resolved exactly are not feasible. Moreover, a detailed description of the *micro-scale* is seldom available and reduced or simplified models where *micro-scale* features are upscaled are therefore of interest. For instance, the numerical method developed in Paper A and B

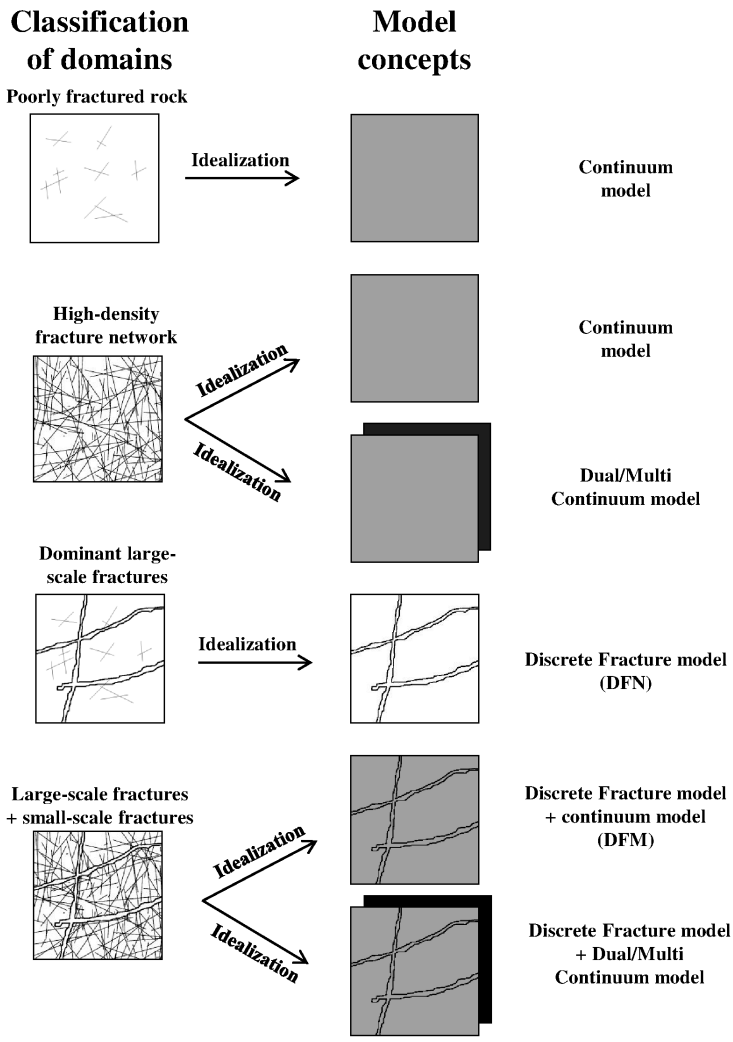

Figure 1.4: Macro-scale modeling concepts

aims to discretize a *macro-scale* model, where *micro-scale* features i.e. the *small-scale fractures* are upscaled. Also the upscaled transport models presented in Paper D and E can be considered *macro-scale* models. Here a numerical upscaling of *micro-scale* parameters are conducted to compute the *macro-scale* parameters, and thus creating a one-way link from the *micro-scale* to the *macro-scale* model. Furthermore, a computational grid with a resolution in-between the *micro-* and *macro-scale* is used to represent the *small-scale fractures* and to resolve *micro-scale* processes more accurately.

The modeling concepts depend on the characteristics of the fractured porous media. Based on the discussions in [16, 28], four different problem types are classified and the corresponding conceptual models suggested. These concepts are shown in Figure 1.4. The first case considers a poorly fractured rock, for which appropriate averaged properties can be defied for the *micro-* and *meso-scale* features, resulting in a single continuum description of the media. If the case involves a dense network of fractures as in the second example, a continuum description may still be appropriate. If the fractures are small and poorly connected a single-continuum model is sufficient, but if the fractures are large and well-connected, distinguished continua must be used for the fractures and the porous media. This is the classical dual continuum model pioneered by [12]. From the discussion of time-scales, it is evident that thermal equilibrium may not always be assumed locally within the porous medium at the *macro-scale*. A remedy is sub-gridding models (MINC models) as suggested by [88], or numerically upscaled MINC type models as suggested in [20, 27, 39, 53, 69]. This concept can further be extended to include cases with fractures at more than one scale by representing the fractures in separate continua based on their scales, in so-called multi-continuum models [28]. Note however that a strict scale separation is needed between the different continua for the models to be mathematically consistent. An alternative but related approach is the upscaled transport models presented in Paper D and E. In contrast to the MINC type models discussed above, where the same *macro-scale* grid is used both for the flow and the transport equation, different levels of coarsening can be applied to the equations in the approach used in these papers. This is often an advantage as flow and transport equations have fundamentally different characteristics.

The third case consists of a network of *large-scale fractures* that dominates the system. The matrix flow can in such cases be neglected and flow in fractures modeled using Discrete Fracture Network (DFN) models [95]. The forth case also consist of a few *large-scale fractures* that dominate the system, but in contrast to Case 3, the flow in the *small-scale fractures* and the porous media cannot be neglected in this case. For the fourth case a Discrete Fracture Matrix (DFM) model must be used, where the *large-scale fractures* are represented explicitly in the model, while the *small-scale fractures* and the porous media are upscaled into continua. Examples of applications of such models are for instance found in [47, 64, 85]. The discrete fracture model can also be combined with dual-continuum models as shown by [85] or MINC type models as shown in Paper D and E.

The four cases considered here describe more or less idealized situations; in nature such idealized cases seldom exist. Most profound is the assumption of a clear separation of scales, both in terms of the spatial extent and in the flow properties underlying all of these simplified models. As a result, modeling errors due to cut-offs may be severe, and worse, the possibility of quantifying or controlling these error is not often possible. An alternative approach, where the modeling error can be controlled to a

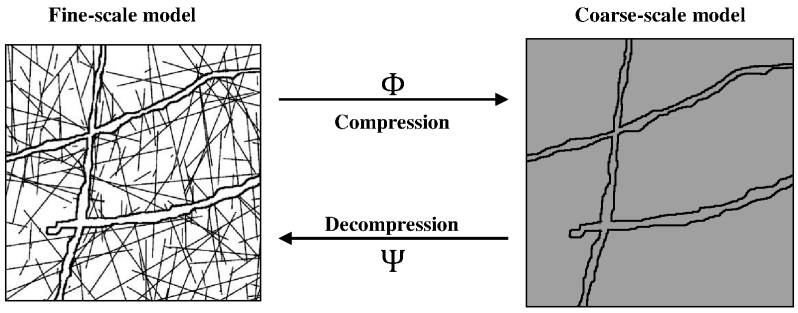

Figure 1.5: Multiscale modeling concepts

larger extent, is based on multiscale modeling.

1.4 Multiscale models

In cases where an appropriate *macro-scale* model cannot easily be defined, accessing the finer scales may be inevitable. Multiscale modeling provides a framework for moving between the scales based on the idea that the same physical phenomena are represented at more than one scale in the same model. The multiscale concept is illustrated in Figure 1.5.

There are two types of multiscale approaches based on whether the rescaling is done prior to the numerical discretization or within it. The vertical equilibrium model for CO_2 storage described in [82] is an example of the first type. Here the vertical dimension is compressed into a two-dimensional coarse model by assuming free CO_2 and brine to be in equilibrium at the relevant time-scales. An example of the second type is the multiscale approach for fractured reservoirs found in Paper C, D and E. Only the second type will be considered in this thesis.

The first step in constructing multiscale models applicable for fractured porous media, is to identify the scales that cannot be upscaled. Based on the discussions related to scales done earlier in this chapter, *micro-scale* effects do not need to be resolved, and therefore only the *meso-* and the *macro-scale* needs to be represented in the model. For convenience the model description on the *meso-* and *macro-scale* will be referred to as the fine- and coarse-scale model, respectively. In cases where either *micro-scale* effects cannot be upscaled or the lateral extend of the reservoir is much larger than what is used here, it may be beneficial to involve more than two scales in the model description. This is however not considered at this stage, but discussed further in Chapter 4.2.2.

The second step is to define the coarse-scale model. Most numerical multiscale models in the literature consider Cartesian fine and coarse grids. With Cartesian grids, the coarse-scale model typically consists of equally distributed sample points (fine-scale cells) representing the system in its nearby cells. Ideally the coarse model should represent the dominant large-scale features. For fractured porous media the long-range correlations are explicitly given by the *large-scale fractures*. An ideal candidate for

the coarse-scale model is thus the discrete fracture matrix (DFM) model suggested for Case 4 earlier, where only the *large-scale fractures* are represented explicitly in the coarse grid. Such coarse grids are further studied in Paper C and D.

The third step is to define compression (Φ) and reconstruction operators (Ψ) that can be used to move between the scales. The compression operator reduces the number of unknowns by mapping the fine-scale to the coarse scale, while the reconstruction operator takes information from the coarse scale and maps it down to a fine-scale. As the motivation for multiscale models is to gain efficiency compared to solving the problem on the finest scale and accuracy compared to solving the problem on the coarsest scale, these operators often involve some degree of approximations. These approximations are based on modeling assumptions often only strictly valid in limiting cases. As these underlying assumptions become more and more questionable, the modeling error will increase, and distort the multiscale solution.

The multiscale method presented in Paper C, D and E is based on the multiscale finite-volume method introduced in [49]. Here the compression operator consists of piecewise constant test functions associated with a coarse primal grid. This particular choice of the compression operator asserts a locally conservative coarse discretization i.e. a coarse finite-volume discretization. The reconstruction operator consists of a set of basis functions associated with each of the coarse variables. These basis functions are computed numerically by solving localized flow problems. To determine the boundary conditions for the localized problems, lower-dimensional problems are typically solved at the boundaries. By neglecting flow normal to the boundaries, the local problems are decoupled, and solved efficiently in parallel. For fractures media, the limiting case where such assumptions are valid is the case where a discrete fracture network model can be used (Case 2). That is when flow in large- scale fractures dominates such that flow in the porous media can be ignored. As flow in the *small-scale fractures* and the porous media become more important the quality of the coarse model degenerates. The remedy is then to apply the coarse model as a preconditioner in an iterative liner solver for the fine-scale problem as further discussed in Paper D and in Chapter 3.3.3.

Chapter 2

Mathematical models

make everything as simple as possible,
but not simpler
Albert Einstein

This chapter presents a set of equations describing heat and mass transfer in fractured porous media. Central to the derivations are the principles of conservation of mass, momentum and energy. The mathematical equations are defined on what was termed the *meso-scale* in Chapter 1.1. For flow in pores and thin fractures, these *meso-scale* equations are often adequate. For wide and open fractures the effect of *micro-scale* features as the roughness of the fracture surface and the fluid-rock interface play a larger role. In such cases the Navier-Stokes equation defined on the *micro-scale* for the void space in individual fractures describes the fluid flow more accurately. But as discussed in the previous chapter, *micro-scale* features and phenomena cannot be fully resolved in field scale simulations. An alternative is to use *micro-scale* equations for fluid flow in the *large-scale fractures* only and *meso-scale* equations for the rest of the domain. Such multiscale approaches will not be followed herein. Instead the same mathematical equations are used to describe heat and mass transport in all fractures and pores.

The *meso-scale* equations can be derived from associated *micro-scale* equations with some additional assumptions. Herein, we instead focus on the derivation of the simplified model equations used in the included papers. In particular, this means that the discussion is limited to single phase flow. Extensions to multiphase fluid flow, including phase changes, are further discussed in Chapter 4. For a general treatment of multiphase fluid flow in porous media and the derivation of the *meso-scale* equations we refer to the following text books [14, 23, 25, 55].

2.1 Rock parameters

A porous media consists of channels and isolated pockets of pores where fluid can be present and a solid part. The solid part is typically referred to as the matrix. A detailed description of the structure and shape of individual pores is not available and the porous media is therefore treated as a continuum, where the macroscopic parameters are defined on what is called a representative elementary volume (REV). A REV is the smallest volume where invariant locally averaged parameters can be defined [14].

The REV must be large enough to include several pores in order to not depend on the *micro-scale* structure of individual pores, and at the same time small enough to exclude large scale heterogeneities in the media. We will assume that a REV can be defined on the *meso-scale*.

2.1.1 Porosity

The ratio of the total pore volume in a REV to the total volume of the REV defines the porosity (ϕ) of the medium. In practice it is more common to use the effective porosity, where the non-connected pores are excluded from the pore volume. Hereafter, the term porosity is used for the effective porosity. The porosity of sand can be as large as 40%, while for sandstone it typically varies between 10% and 20% [14]. For solid granite the porosity may be less than 1%, but in cases where the rock is fractured the porosity increases notably. For instance in the geothermal EGS site in Soultz the porosity varies between 0.3% and 10%, depending on the fracture density [102]. The porosity changes as a result of internal stress caused by the fluid pressure, external stress from the formation or through chemical reactions. Components in the fluid may for instance precipitate and narrow or plug pores, or chemically react with the solid (corrosion) to increase the pore space. Such effects are not considered herein, but further discussed in the context of combined THMC models in Chapter 4.3.

2.1.2 Rock permeability

The rock permeability (**K**) is a measure of the porous media's ability to conduct flow. The permeability is related to the porosity and the tortuosity of the pores, but as the exact structure of the pores is not known, the permeability is mostly determined experimentally. For instance permeability values of around 10^{-16} m^2 in the surrounding rock and 10^{-13} m^2 in the stimulated (fractured) rock are reported in the Geothermal EGS site in Soultz [60]. The porous media is anisotropic and therefore best described by a tensor. From Onsager's principle it follows that the permeability tensor is symmetric and positive definite [14]. In the previous chapter tensor permeabilities was introduced to represent the *small-scale fractures* in a *meso-scale* model. In general the anisotropy can also have other sources and it is therefore important that the discretization handle symmetric and positive definite tensors. The numerical method presented in Paper A and B discretize tensor permeabilities consistently also for general grids.

2.1.3 Fracture permeability

In cases where the fractures are filled they can be considered as a porous medium and the above definition of rock permeability can be applied directly. For open fractures the notion of permeability is somewhat different. As discussed in the introduction, flow in open fractures can be described using the Navier-Stokes equation or the Stokes equation in case of creeping flow with negligible inertial forces. If further the fractures are assumed to be locally described by parallel plates, such that the normal velocity can be neglected and the shear forces acting normal to the fracture wall dominate, a *meso-scale* equation for flow in a single fracture can be derived [28]. This *meso-scale* equation is often referred to as "the local cubic law" as the magnitude of the fluid flow

is proportional to the cube of the local aperture. Based on "the local cubic law", an equivalent fracture permeability can be defined, that is

$$k_f = \frac{a^2}{12}, \tag{2.1}$$

where a is the local aperture [28]. Although "the local cubic law" is widely used to describe flow in single fractures its underlying assumptions are often questionable as further discussed in for instance [16]. The expression for the fracture permeability in (2.1) is applied for open fractures in Paper C, D and E, while Paper A and B assume that the fractures are filled and can be considered a porous media.

2.2 Fluid properties

The fluid properties vary with pressure (p) and temperature (T) by what is called equation of states. Depending on the pressure and the temperature, a fluid can exist in different phases. As the fluid properties change drastically when a fluid change phase, a change of phase has a significant impact on the fluid flow. The examples found in the included papers are mostly concerned with liquid water. Many of the simplifications utilized in the mathematical models herein are based on assumptions valid for liquid water, and not for steam or CO_2. In natural hydrothermal reservoirs the present fluid is water often with some amount of dissolved or free CO_2 and other chemical species. Also, the high temperatures found at relatively shallow depths in many hydrothermal reservoirs leads to the water being in a gas phase here. Many of the simplifying assumptions underlying the mathematical models presented herein are therefore not in general valid for such cases. Necessary extensions are further discussed in Chapter 4.

2.2.1 Density

The density (ρ) is the amount of mass per volume. The change in density can be related to change in temperature and pressure by the thermal expansion coefficient (α) and compression coefficient (β), respectively. By expanding the change in density in terms of pressure and fluid temperature, an expression for α and β can be obtained:

$$\frac{\partial \rho}{\partial t} = \frac{\partial \rho}{\partial T}\frac{\partial T}{\partial t} + \frac{\partial \rho}{\partial p}\frac{\partial p}{\partial t} = \rho\left(-\alpha\frac{\partial T}{\partial t} + \beta\frac{\partial p}{\partial t}\right). \tag{2.2}$$

The thermal expansion coefficient and the compression coefficient depend on the pressure and the fluid temperature. For water in liquid state the compression coefficient and the thermal expansion coefficient are small, and water can be considered incompressible. As the thermal expansion coefficient increases with temperature, these assumptions are only valid for small temperatures.

2.2.2 Viscosity

Flow can be described as a continuous deformation of a fluid in the presence of shear stresses. The viscosity (μ) is the property of the fluid to resist such deformations. For example highly viscose fluids as honey move slower than the less viscose water,

given the same pressure gradient. The viscosity of the fluid depends strongly on the temperature, but is more or less insensitive to changes in pressure. Viscosity is therefore often regarded as a function of temperature only.

2.2.3 Internal energy, enthalpy and heat capacity

For the thermo-dynamical properties to be scale invariant, the following intensive quantities are used: Specific internal energy (e), specific enthalpy (h) and specific heat capacities (c_p, c_V). The specific internal energy of a system is the total energy contained in the system. The internal energy includes both the kinetic and the potential energy, but not the energy needed to displace the environment in order to make room for its volume (V) and pressure. The specific enthalpy equals the internal energy and the energy that is transferred to the environment through the expansion of the system: $h = e + p/\rho$. For fluids in gas phase, enthalpy is therefore the preferred variable for the system energy. The SI unit for specific internal energy and specific enthalpy is J/kg.

The heat capacity relates the amount of heat needed to change the temperature of the medium. For constant pressure the specific heat capacity equals the change in specific entropy per temperature:

$$c_p = \left(\frac{\partial h}{\partial T}\right)_p. \tag{2.3}$$

The subscript p is used to distinguish the heat capacity under constant pressure conditions with the heat capacity under constant volume conditions. The heat capacity under constant volume conditions equals the change in specific internal energy per temperature:

$$c_V = \left(\frac{\partial e}{\partial T}\right)_V. \tag{2.4}$$

The difference between the heat capacities is related to the thermal expansion coefficient and compressibility coefficient. $c_p - c_V = (\alpha^2 T)/(\rho\beta)$ [61]. For liquid water the compression coefficient is small and the two heat capacities are almost identical.

2.3 Fourier's law and the thermal conductivity

Fourier's law states that the heat transfer ($\mathbf{v_T}$) in a medium is proportional to the temperature gradient:

$$\mathbf{v_T} = \lambda \nabla T, \tag{2.5}$$

where the proportionality constant λ is the thermal conductivity of the medium. The thermal conductivity is a measure of the materials ability to conduct heat. Granite is for instance a poor heat conductor compared to iron. The thermal conductivity however varies in a much smaller degree than the permeability [55]. The SI unit for thermal conductivity is W/(mK).

2.4 Darcy's law

An equation relating the macroscopic fluid velocity ($\mathbf{v}$) to the difference in hydraulic head was first described by Darcy in 1856 and later generalized to the following expression referred to as Darcy's law for single phase flow:

$$\mathbf{v} = -\frac{\mathbf{K}}{\mu}(\nabla p - \rho g \nabla z). \tag{2.6}$$

Here g and z are used for the gravitational constant and the depth, respectively. Under certain assumptions, Darcy's law can be shown to be consistent with a locally averaged Navier-Stokes equation defined on the *micro-scale* [112], but in the general case additional terms are needed in Darcy's equation to fully describe the flow.

Of special importance for flow in fractured porous media is the Forchheimer correction. In the case of fast flow, for instance in fractures, the *micro-scale* inertia effects cannot be ignored and a friction term appears in Darcy's equation;

$$\mathbf{v} = -\frac{\mathbf{K}}{\mu}(\nabla p - \rho g \nabla z) - \mathbf{F} \cdot \mathbf{v}, \tag{2.7}$$

where $\mathbf{F}$ is the Forchheimer correction tensor. For simplified geometries and small velocities, $\mathbf{F}$ can be shown to have a linear dependency on the velocity $\mathbf{v}$ [112]. Only Darcy's law is considered herein, but inclusion of the Forchheimer term in the proposed methods is discussed in Chapter 4.

2.5 Flow and mass transport

According to the principle of mass conservation, the accumulated mass within an arbitrary volume Ω must equal the total mass influx over the boundary $\partial\Omega$ plus any contribution from a source term within the volume. Mathematically this can be expressed as

$$\int_\Omega \frac{\partial}{\partial t}(\phi\rho)\, \mathrm{d}\Omega = -\int_{\partial\Omega} (\rho \mathbf{v}) \cdot \mathbf{n}\, \mathrm{dS} + \int_\Omega q\, \mathrm{d}\Omega. \tag{2.8}$$

Here, $\mathbf{n}$ is the outward unit normal (hence the minus sign before the flux expression) and q is the mass source term. By applying the divergence theorem to convert the boundary integral to a volume integral and recognizing that the integral equation is valid for an arbitrary volume, the integrals can be removed. The mass conservation equation can thus be written on differential form:

$$\frac{\partial}{\partial t}(\phi\rho) + \nabla \cdot (\rho \mathbf{v}) = q. \tag{2.9}$$

In general ρ, μ and ϕ depends on temperature and pressure. The differential equation in (2.9) is thus both nonlinear and parabolic.

2.5.1 The pressure equation

We will now derive the simplified equations used in the included papers. Assuming that the effects of the mechanical and the chemical processes on the porosity are small, the compressibility of the rock can be assumed to be order of magnitudes smaller than that of the fluid. Equation (2.9) can in such cases be simplified to

$$\phi \frac{\partial \rho}{\partial t} - \nabla \cdot \left(\frac{\rho}{\mu} \mathbf{K} (\nabla p - \rho g \nabla z) \right) = q. \tag{2.10}$$

Here Darcy's equation in (2.6) is applied to equation (2.9) in order to express the equation in terms of the pressure.

For small temperature and pressure variations, the fluid can often also be assumed to be incompressible and an elliptic equation (in terms of pressure) models the flow

$$-\nabla \cdot \left(\frac{\mathbf{K}}{\mu} (\nabla p - \rho g \nabla z) \right) = \frac{q}{\rho}. \tag{2.11}$$

Water can be considered incompressible under normal pressure and temperature conditions, but in the gas phase water is highly compressible and the above simplification fails. Understanding the properties of this standard elliptic equation is still important also for the more general flow problem as the differential equation preserves most of its elliptic character even in the case of compressible fluids and rocks. Equation (2.11) is applied in Paper B-E, while Paper A considers the more general compressible case. The discretization of the elliptic equation is considered in Chapter 3.3.

2.5.2 The linear transport equation

Paper A-D is mainly concerned with solving the pressure equation. A good metric to gauge the pressure solution is to apply it to a transport equation and compare the integrated solution found in the production wells. The simplest transport equation considers advection of a passive tracer present in the fluid phase, which can be described by the linear transport equation;

$$\phi \frac{\partial \tau}{\partial t} + \nabla \cdot (\tau \mathbf{v}) = q^{\tau}. \tag{2.12}$$

Here τ is the concentration of the tracer and τ_c the volumetric source term. The transport equation is a hyperbolic differential equation and its discretization is presented in 3.4.

2.6 Heat transport

A heat transport equation can be derived from the principle of energy conservation [55]. Energy flows freely between the solid and the fluid phases, and the derivation of a conservation equation for energy on the *meso-scale* from the first principles is not as straight forward as for the mass, where we simply can assume that all fluid mass is contained within the pore space. A local volume averaging technique is applied in

[55] to derive equations on the *meso-scale*. The derived equations include terms depending on the interfaces between the fluid and the solid, simplifications are therefore inevitable. Two such simplified models are considered here. In the first model local thermal equilibrium between the solid and the fluid is assumed. Based on the discussion of temporal scales in 1.2, this is a reasonable assumption. A temperature equation where local equilibrium is assumed, is applied in Paper A and E. In Paper G, a model where local thermal equilibrium is not assumed is considered. In this model the interaction between the phases is modeled by a single heat transfer coefficient.

2.6.1 The temperature equation

In the case where the temperature difference between the solid and the fluid in a REV is in order of magnitudes smaller than the temperature difference in the system, the system is close to a local thermal equilibrium. If local thermal equilibrium can be assumed, and the radiation and the kinetic energy neglected, the energy balance equation reads: [25, 111]

$$\frac{\partial}{\partial t}\int_{\Omega}\left[(1-\phi)(\rho_s e_s)+\phi(\rho_f e_f)\right]\mathrm{d}\Omega + \int_{\partial\Omega}\left[(\rho_f h_f)\mathbf{v}-\boldsymbol{\Lambda_e}\nabla T\right]\cdot\mathbf{n}\,\mathrm{dS}=q^e. \tag{2.13}$$

Here the subscript s and f stands for solid and fluid, respectively, and q^e is the energy source. An effective thermal conductivity $\boldsymbol{\Lambda_e}$ is used to describe the combined heat conduction in the fluid and solid. The effective thermal conductivity depends on the structure of the solid matrix and the thermal conductivity of the solid and the fluid. For simple geometries with periodic structures the effective thermal conductivity can be determined analytically, but in practice the effective thermal conductivity is determined experimentally [55]. While the thermal conductivity of the solid and fluid on the *micro-scale* is a scalar (2.5), a full tensor is needed in order to describe the thermal conductivity on the *meso-scale*.

In the unsaturated case where only one phase is present, it is convenient to use the temperature as one of the primal variables in addition to the pressure, as the temperature can be measured directly in contrast to enthalpy or internal energy. In the saturated case where two phases coexist, temperature and pressure are directly related and they cannot both be used as primal variables. One option is to use pressure and saturation of one of the phases as primal variables [25, 87], or alternatively pressure and enthalpy. In both cases a saturated steam table must be used to determine the secondary variables.

A simplified equation for temperature can be derived from the energy equation by assuming the heat capacity and density to vary slowly with time:

$$(\rho c_p)_e\frac{\partial T}{\partial t}+(\rho c_p)_f\nabla\cdot(T\mathbf{v})-\nabla\cdot\boldsymbol{\Lambda_e}\nabla T=q^e, \tag{2.14}$$

where the subscript e is used to denote effective parameters and q^e is the energy source term. The effective heat capacity is simply:

$$(\rho c_p)_e=\phi(\rho c_p)_f+(1-\phi)(\rho c_p)_s. \tag{2.15}$$

For liquid water these assumption are appropriate, but in the general case where a gas phase is present, the above simplifications cannot be made. The applicability of the methods developed in this thesis for more general cases are further discussed in Chapter 4.

The temperature equation in (2.14) includes both a convective and a conductive term. The different character of the convective and conductive terms must be taken into account when numerical discretizations are considered for the temperature equation as further discussed in the next chapter.

2.6.2 The non-equilibrium temperature equation

In cases where local thermal equilibrium cannot be assumed, the complex heat transfer between the phases is often modeled by a simple heat transfer coefficient h_{sf}. One such model that is applied in Paper G is [55]:

$$(1-\phi)(\rho c_p)_s \frac{\partial T_s}{\partial t} = \nabla \cdot (\mathbf{\Lambda_s} \nabla T_s) + (1-\phi) Q_s^e - h_{sf}(T_s - T_f), \tag{2.16}$$

$$\phi(\rho c_p)_f \frac{\partial T_f}{\partial t} + (\rho c_p)_f \nabla \cdot (T_f \mathbf{v}) = \nabla \cdot (\mathbf{\Lambda_f} \nabla T_f) + \phi Q_f^e + h_{sf}(T_s - T_f). \tag{2.17}$$

Here the effective thermal conductivities of the solid and the fluid, as well as the heat transfer coefficient, must be determined experimentally. This simplified model cannot account for the complex heat exchange occurring between the phases. As a result all neglected terms are included in the single h_{sf} coefficient and experimental values from one model cannot automatically be used for other models.

Chapter 3

Numerical discretization and solution strategies

Computers are incredibly fast, accurate and stupid.
Human beings are incredibly slow, inaccurate and brilliant.
Together they are powerful beyond imagination.
Unknown

In the previous chapter, mathematical equations for fluid flow and heat transfer in porous media were presented. Analytical solutions to these equations can be found for some simplified cases, but in general numerical solutions must be sought. In this chapter, numerical methods and solution strategies for solving the model equations presented in the previous chapter are presented. The pressure (2.11), temperature (2.14) and linear transport (2.12) equations presented in Chapter 2 are coupled, time depended, and possibly non-linear. These issues must be dealt with by the numerical methods. Moreover, the different equations have different characteristics. The pressure equation has an elliptic character. This applies even for the slightly compressible case, where the equation is formally parabolic, but where the elliptic behavior often dominates. Similarly, the tracer transport equation has a hyperbolic character, while the temperature equation includes both a hyperbolic and an elliptic term. The different properties of the elliptic and hyperbolic terms motivate using different discretization techniques.

The numerical methods developed in Paper A-D are mainly focused on the discretization of the elliptic equation. In Paper B, the discretization of the hyperbolic equation is also considered, when a single-point upstream method is extended in order to handle intersecting fractures. Furthermore, in Paper D and E, flow-based upscaling is introduced for the hyperbolic equation in order to gain efficiency compared to fine-scale models. In this chapter elliptic and hyperbolic discretization techniques are presented separately with particular emphasis on the methods developed in these included papers. Strategies for time-integration, coupling and non-linearity are thus only briefly discussed in the beginning.

A matter not discussed so far, but nevertheless important when fractured reservoirs are considered, is the construction of the computational grid. A whole section in this chapter is thus devoted to this particular challenge. The gridding is highly related to both the conceptualization and the numerical discretization of the fractured reservoir and must therefore be discussed as a whole. The multiscale approach developed for fractured reservoirs in Paper C-E considers not only one computational grid, but a

hierarchy of grids. For these methods to be applicable for complex fracture geometry, an efficient and robust gridding algorithm is crucial.

3.1 Coupling strategies, time-stepping and non-linearity

How the coupling of the equations, the evolution of time and the non-linearities are handled are related. A full analysis of these integrated issues is beyond the scope of this thesis, for further details we refer to [11, 25]. Here, we only present the background for the choices made in the included papers.

Different simulation strategies are formulated based on which terms that are treated implicitly and which terms that are treated explicitly. In commercial simulators, fully implicit strategies are often preferred due to their robustness [1, 87]. The fully implicit method is computational intensive as large systems of non-linear equations must be solved at each time-step. A more flexible, often less time consuming and simpler strategy is to decouple the equations and solve them in sequel. Different discretizations and time-stepping strategies suited for each of the equations can then be used. The pressure variable is always treated implicitly due to the global dependency of the elliptic equation, while mass (or concentrations) are often treated explicitly to reduce the computational cost and the numerical dispersion. Sub time-steps can be applied for the mass transport equation to meet time-step restrictions associated with the explicit methods [67]. The temperature can either be treated implicitly or explicitly depending on whether convection or conduction dominates. The decoupling introduces a splitting error that may be severe in cases with highly non-linear couplings. The remedy is to iterate a few times before moving to the next time step. A more robust approach that combines the benefits of both these strategies, is the adaptive implicit method where the "problematic" cells are solved implicitly, while the rest are solved explicitly [106]. Due to its robustness and the presence of small fracture cells, implicit methods are chosen in all the included papers, except in Paper A, where pressure and temperature are treated implicitly and mass explicitly.

To solve the non-linear equations, iterative methods as the Newton-Raphson scheme is used. For good initial guesses, often just the solution at the previous time-step, the Newton-Raphson scheme converges after a few iterations. But in cases where the non-linearity is strong, the scheme may not converge at all. In situations where the Newton-Raphson scheme fails, a new attempt can be made with a reduced time-step. For each of the iterations a linear system is solved. This implies that a very large number of linear systems are solved during a simulation. For large reservoir simulations as much as 80-90% of the computational time can be spent on solving linear systems [25]. Developing efficient linear solvers for reservoir simulations is therefore crucial.

The large number of unknowns present in realistic reservoir models favors iterative Krylov methods as CG [42], GMRES [94] and BiCGSTAB [100]. The efficiency of the Krylov methods is improved by applying preconditioners. For elliptic equations, multi-grid with domain decomposition preconditioners are favorable [15, 101, 107], while local methods as iLU(0) factorization are often used for the hyperbolic equations [25]. An efficient two-level preconditioner for the elliptic equation tailored to fractured porous media is presented in Paper C and D.

3.2 Gridding algorithms for discrete fractures

As discussed in the introduction of this chapter, the gridding of fractures is related to how the fractures are modeled conceptually and the type of discretizations used. The quality of the grid will also directly influence the accuracy obtained by the discretizations.

Conceptually, fractures can either be modeled as lower-dimensional objects, i.e. lines in 2D and planes in 3D, or with the same dimension as the grid cells used to represent the porous media. An advantage with an equi-dimensional representation of the fractures is that standard discretization schemes can be applied directly without modifications. From the discussion of spatial scales in Chapter 1, it is clear that resolving the fracture aperture geometrically in a *mega-scale* model is not desirable. On the *meso-scale* fractures are therefore conceptually modeled as lower-dimensional objects. The gridding is simplified with a lower-dimensional representation of the fractures and, moreover, the introduction of small elements in the intersection of fractures in equi-dimensional models significantly degrades the quality of the grid, which further motives using lower-dimensional models for the fractures.

Along with what is done in the included papers, we will only consider cases where the fracture grid conforms to the rest of the grid. This implies that the fractures act as constraints in a tessellation with for instance triangles in 2D or tetrahedra in 3D. An alternative approach that circumvents the need for the constrained tessellation and reduces the number of unknowns significantly, is to embed the fractures into coarser grid cells [22, 44, 64, 116]. These non-conforming methods are based on simplifying assumptions on the matrix-fracture interaction, and they are not persuaded further in this thesis.

The geometric complexity of fracture networks makes gridding a major challenge for standard discrete fracture models. In [91] four challenging configurations for the grid generator are identified:

1. Slightly intersecting fractures.
2. Almost intersecting fractures.
3. Close and nearly parallel fractures.
4. Fractures intersecting at very small angles

If these cases are honored precisely, they introduce very small cells or cells with very small or very large angles. For instance, the conventional Delaunay approach [99] will refine the grid extensively around the problematic configurations and create very small cells. In addition to introducing a large number of cells, the quality of the grid is often such that a large discretization error is inevitable. In other words there is a tradeoff between honoring the fracture geometry precisely and the quality of the grid, and thus also the accuracy of the discretization. We will now present some approaches that are developed to improve the quality of the grid. The key ideas are to relax the accuracy of the fracture representation to avoid the challenging cases identified in [91] and to massage the resulting grid to remove small and distorted cells.

In [43] the quality of the constraint grid is improved by assigning forces between nodes on either sides of the edges, and move the nodes until a global force-equilibrium

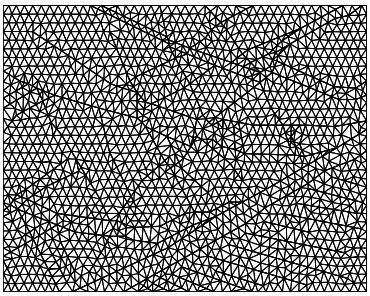

Figure 3.1: Triangulation constrained by the outcrop in Figure 1.2 (From [43]).

is obtained. An example of a grid computed using this method, constrained by the outcrop shown in Figure 1.1, is shown in Figure 3.1. The method in [43] honors the fractures geometries exactly. In [73] the requirement of honoring the fracture geometry is relaxes. By specifying a grid resolution so that features smaller than the given resolution is not resolved, the quality of the grid is improved considerably. This means that fractures localized close to each other are snapped together or slightly moved, possibly creating non-physical connections between the fractures. But taken into account the large uncertainty in the geometry and location of the individual fractures, such relaxation seem reasonable.

The algorithms in [43, 99] are restricted to two spatial dimensions. The algorithm in [73] has some 3D features that allow for genuine 3D grids, but for the moment it is restricted to handle 2D fracture networks that are extended in the vertical direction. The algorithm presented in [77] is demonstrated for both 2D and 3D fracture networks. A key idea in this work is to systematically remove bad quality grid cells (small in size or angles) from the grid by merging nearby cells. Still gridding a full 3D fracture network that possess good grid quality remains a challenge.

The actual gridding time for 3D grids and large 2D grids with a large number of fractures may become severe as the gridding time follows a quadratic law with respect to the number of vertices in the grid [7]. According to [7], considerable efficiency can be gained using a domain decomposition strategy, where the grid is partitioned into subdomains and gridded locally. Such domain decomposition strategies fit nicely with the construction of the multiscale grid hierarchy and is implemented for the two level grids found in Paper C-E.

3.3 Elliptic discretizations

The pressure equation in (2.11) and the temperature equation in (2.14) include elliptic terms. These terms can be discretized in a similar way, and only the elliptic pressure equation will therefore be considered herein. Recall the elliptic pressure equation as stated in (2.11):

$$-\nabla \cdot (\mathbf{K}\nabla p) = q. \tag{3.1}$$

For readability unit viscosities and densities are used that is, $\mu = 1$ and $\rho = 1$. Here p still is used for the pressure, $\mathbf{K}$ for the permeability tensor and q for the source term.

From the theory of elliptic differential equations [31], the elliptic operator is known to be symmetric, positive definite and fulfill the maximum principle for sufficiently regular $\mathbf{K}$ and q. It is desirable that the discretization preserves these properties. The maximum principle guarantees that no spurious oscillations occur in the interior of the domain for the solution of (3.1) and a discretization method that obeys the maximum principle is called monotone. Another important property is local conservation. In particular, if velocities obtained from the solution of (3.1) are used in hyperbolic conservation laws, a non-conservative method may lead to unphysical solutions [66]. Examples of conservative schemes used in reservoir simulations are; mixed finite element [25], discontinues finite element [23], control-volume finite element [22], mimetic finite difference [19, 68] and finite- volume methods [4, 29]. Lower-dimensional fracture representations have also been developed within most standard discretizations: Finite-volumes; Paper A, B and [52], control-volume finite elements [13, 75, 90], mixed finite elements [9, 74] and mimetic methods [79]. Our emphasis is on the finite-volume methods as these are the standard in reservoir simulators [87, 98].

The elliptic equation has a global domain of dependence, meaning that a local change in one cell is felt instantaneously in the whole domain. When discretized, the elliptic equation renders a globally coupled and thus expensive set of algebraic equations to solve. From the discussion of scales and conceptual models in Chapter 1, it is clear that a fully resolved *meso-scale* model is not always feasible, and that instead upscaled or multiscale solutions must be sought.

The first part of this section is concerned with the finite-volume discretizations for standard cells and lower-dimensional fracture cells as addressed in Paper A and B. In the second part the multiscale finite-volume method [49] is presented with an emphasis on its adaption to fractured reservoirs as proposed in Paper C and D. For other multiscale methods we refer, for instance, to [30, 46] for the finite element approach, [24] for the mixed finite elements approach and [2] for the mimetic approach.

3.3.1 Finite-volume discretizations

A finite-volume formulation of (3.1) is obtained by integrating the equation over each cell Ω_j and using the divergence theorem,

$$\int_{\partial\Omega_i} (\mathbf{v}\cdot\mathbf{n})\,\mathrm{dS} = \int_{\Omega_i} q\,\mathrm{d}\Omega, \tag{3.2}$$

where $\mathbf{n}$ is the unit normal vector pointing outwards and $\mathbf{v} = \mathbf{K}\nabla p$. The expression in (3.2) is formulated as the conservation law from which it was derived (2.9), implying local conservation in each cell. The volume integral on the right hand side is easily discretized and the main concern is thus the discretization of the flux expression on the left hand side. The flux over each side (S) of a cell can be approximated by the differences in the pressure of the neighboring cells:

$$\int_S (\mathbf{v}\cdot\mathbf{n})\,\mathrm{dS} \approx \sum_{k=1}^{\nu} t_k p_k. \tag{3.3}$$

The number of neighboring cells ν, and the definition of the so-called transmissibility coefficients t_k relating the pressure to the flux, differ between the finite-volume meth-

ods. Assembling the transmissibilities yields a linear system for the equation given in (3.2):

$$\mathbf{Ap} = \mathbf{q}, \tag{3.4}$$

where $\mathbf{A}$ is the discretization matrix, $\mathbf{p}$ is a vector containing the pressures associated with the cells and $\mathbf{q}$ is a vector containing the integrated source contribution in each cell.

A short description of the two-point flux approximation (TPFA) method used in Paper C-F and the multi-point flux approximation (MPFA) method known as the O-method used in Paper A-B and G, now follows. For other commonly used MPFA methods such as the L-method confer [6, 81].

Two-point flux approximation

The simplest and most used scheme is the two-point flux approximation (TPFA) [11]. With a TPFA the flux over a face is assumed to only depend on the pressure in the two adjacent cells. Introducing an unknown at the face center, the gradient can be approximate by the directional derivative of pressure in the direction from the cell centroid to the face centroid. With a half transmissibility, α_i, defined by

$$\alpha_i = \frac{A\mathbf{n}\cdot\mathbf{K_i}}{\mathbf{d_i}\cdot\mathbf{d_i}}\cdot\mathbf{d_i}, \tag{3.5}$$

the flux from cell 1 to cell 2 over the shared edge can be approximated by

$$f_1 = -\int_S \mathbf{n}\cdot(\mathbf{K_1}\nabla p)\,\mathrm{dS} \approx -\alpha_1(\hat{p}-p_1). \tag{3.6}$$

Here A is the area of the shared face, $\mathbf{n}$ is the unit normal pointing from cell 1 to cell 2, $\mathbf{K}_i$ the conductivity in cell i, $\mathbf{d}_i$ is a distance vector from the centroid of cell i to the face center, p_i and $\hat{p}$ is the pressure value in the centroid of cell i and the face center, respectively.

Similarly the flux from cell 2 to cell 1 over the shared edge can be approximated by

$$f_2 = \int_S \mathbf{n}\cdot(\mathbf{K_2}\nabla p)\,\mathrm{dS} \approx -\alpha_2(p_2-\hat{p}). \tag{3.7}$$

The unknown at the face centroid can further be removed by requiring flux continuity, giving the following expression for the flux

$$f_{12} = -t_{12}(p_2-p_1), \tag{3.8}$$

where the transmissibility t_{12} is given by the harmonic average of the half transmissibilities

$$t_{12} = \frac{\alpha_1\alpha_2}{\alpha_1+\alpha_2}. \tag{3.9}$$

For general geometries and anisotropies the TPFA does not yield a consistent discretization of the fluxes. The TPFA scheme is, however, widely used due to its simplicity,

computational efficiency and robustness, as the TPFA always gives a discretization matrix that is monotone, symmetric and positive definite.

Only when the anisotropy aligns with the grid, that is when $\mathbf{n} \cdot \mathbf{K} \parallel \mathbf{d}$, a TPFA is consistent. Grids where the above property holds are called K-orthogonal. As geological structures like layers and fractures constrain the grid, using K-orthogonal grids are not always possible and multipoint schemes must be applied.

Multipoint flux approximation

A class of different multipoint flux approximation (MPFA) methods that yield a consistent discretization of the flux for general anisotropies have been developed during the last decades. The MPFA schemes give a larger cell stencil than the TPFA scheme and are therefore more computational expensive. Moreover, while the TPFA scheme is unconditional monotone, monotonicity is not always guaranteed for the MPFA methods. In fact, it is shown that no unconditionally monotone method which also reproduce linear potential fields exactly, and have local conservation can be constructed [81]. As a remedy, different MPFA schemes with different monotonicity conditions and cell stencil sizes are derived. The original and most used MPFA scheme is the O(η)-method [4, 29], where a parameter η is used to specify the location of the continuity point at the interface. If the centroid of the face is used as the continuity point ($\eta = 0$) the method gives a TPFA scheme for K- orthogonal grids. For triangular grids, $\eta = 1/3$ is a optimal choice [35, 56]. Convergence studies for the MPFA-O method conducted in for instance [5, 57] indicate second order convergence for the pressure and first order for the flux for sufficiently smooth solutions.

To construct the MPFA O-method, we consider an interaction region for each vertex in the domain. The interaction region is constructed by connecting the cell centroids of all the cells sharing the vertex with their corresponding face centroids. In each cell in the interaction region, the pressure is assumed to be linear; that is,

$$p(\mathbf{x}) = \sum_{k=1}^{m+1} p_k \phi_k(\mathbf{x}), \tag{3.10}$$

where p_k for $k \neq 0$ is the pressure in the m continuity points, p_0 is the pressure in the centroid of the cell, and ϕ_k the linear basis function defined by $\phi_k(\mathbf{x}_k) = \delta_{kk}$. Here $\mathbf{x}_k$ gives the location of the discrete pressure points. The flux over the half-face S_j can then be expressed using (3.10):

$$f_j = -\int_{S_j} \mathbf{n} \cdot (\mathbf{K} \nabla p) \, \mathrm{dS} = -\sum_{k=1}^{m+1} A_j \mathbf{n} \cdot (\mathbf{K}_k p_k \nabla \phi_k). \tag{3.11}$$

For each interaction region we obtain a set of half fluxes ($\mathbf{f}$) that can be expressed on the following form:

$$\mathbf{f} = \mathbf{C}\hat{\mathbf{p}} + \mathbf{D}\mathbf{p}. \tag{3.12}$$

Here $\hat{\mathbf{p}}$ and $\mathbf{p}$ are the face and cell pressure, respectively, and $\mathbf{C}$ and $\mathbf{D}$ are matrices relating the pressure to the fluxes. For details of how the coefficients in $\mathbf{C}$ and $\mathbf{D}$ are

calculated, we refer to [4]. Requiring flux continuity over the face results in a set of linear equations of the following form:

$$\mathbf{R}\hat{\mathbf{p}} = \mathbf{S}\mathbf{p}. \tag{3.13}$$

With this equation, the pressure at the faces can be eliminated and we obtain the following expression for the half fluxes:

$$\mathbf{f} = \mathbf{T}\mathbf{p}, \tag{3.14}$$

where the local transmissibility matrix is defined by

$$\mathbf{T} = \mathbf{C}\mathbf{R}^{-1}\mathbf{S} + \mathbf{D}. \tag{3.15}$$

A global transmissibility matrix can now be constructed by adding the local transmissibilities, and further be used to construct the discretization matrix in (3.4).

3.3.2 Finite-volume discretizations for fractures

A finite-volume discretization for lower-dimensional fractures was introduced in [52]. Here fractures are represented by special hybrid cells that are lower-dimensional in the grid, but correctly accounts for the aperture in the computational domain. This hybrid representation avoids troublesome small-cells in the intersection of fractures that put restrictions on the time-stepping in explicit schemes and lead to large condition numbers for the discretization matrix as shown in Paper B. A hybrid representation of fractures is appropriate as long as the aperture is much smaller than the matrix cell size. This corresponds to cases where fractures are conceptually modeled as lower-dimensional objects i.e. the *meso-scale* in our context. For fractures acting as barrier to the flow, this restriction can be relaxed somewhat as shown in Paper B and applied to a study of deformation bands in Paper F.

The hybrid representation implies that modified expressions for fracture-fracture and matrix-fracture transmissibilities accounting for the fracture aperture must be computed. We will briefly discuss these adjustments in the context of the TPFA and the MPFA-O method by focusing on concepts and underlying assumptions rather than the details. For details, including illustrations, confer Paper B and [52].

To account for the fracture aperture in matrix-fracture connections, the continuity point on the face between the fracture and matrix is moved half an aperture away from the fracture. In this way the computational domain mimics the corresponding equi-dimensional representation. For fracture-fracture connections, the fracture aperture is accounted for by defining the area of the face between fractures to equal the aperture in 2D, or the aperture times the length of the face in 3D. To handle intersecting fractures without introducing small-cells in the intersection of fractures, two assumptions are made. First, a constant pressure is assumed in the intermediate cell, which is a reasonable assumption as long as the size of the intermediate cell is small. Second, the accumulation term in the intermediate cells is assumed to be negligible. For single-phase incompressible fluid flow, this assumption is valid as long as no source or sink is placed in the intermediate cell, but also for multiphase and compressible fluid flow this is a reasonable assumption as long as the volume of the intermediate cell is small. With these two assumptions, expressions for fracture-fracture transmissibilities can be

derived for both the TPFA and the MPFA-O method. For the TPFA method this leads to the so-called "star-delta" transformation as presented in [52]. The similar expression for the MPFA-O method is derived in Paper A and B.

3.3.3 The multiscale finite-volume method

The multiscale finite-volume method was introduced in [49]. In the following a short description of the method is presented. The presentation is restricted to two levels, and emphasis is put on its adoption to fractured reservoirs. For a more general description we refer to the original paper [49] and a more recent review paper by [83].

In the multiscale finite-volume method, two sets of coarse grids are used: A coarse primal grid where coarse variables are associated and a coarse dual grid where the basis functions are computed. These basis functions are used to reconstruct the fine-scale variables from the coarse-scale variables as already discussed in Chapter 1.4. The coarse primal grid consists of fine-scale cells that are grouped together into a coarse partitioning of the domain. For each coarse primal cell, one of its fine-scale cells is identified as a coarse-scale variable. In the dual-grid these fine-scale cells are referred to as vertex cells. The dual grid is further constituted by identifying continuous paths of fine-scale cells between the vertex cells which are named edge cells. The edge and vertex cells will now partition the domain. The remaining fine-scale cells are termed interior cells and due to the partitioning, these cells are grouped into disjoint (in terms of the discretization) dual subdomains.

Local problems defined on the dual grid can now be solved to compute the basis functions, where the boundary conditions are given by the solution of a tangential problems along the dual edges [46]. An approximation of the fine-scale pressures $\tilde{\mathbf{p}}^f$ can be computed from the coarse pressures $\mathbf{p}^c$, using the basis functions:

$$\tilde{\mathbf{p}}^f = \boldsymbol{\Psi}\mathbf{p}^c, \tag{3.16}$$

where $\boldsymbol{\Psi}$ is a matrix containing the basis functions in its columns. With the fine-scale approximation of the pressure, corresponding fine-scale fluxes can be computed;

$$\tilde{\mathbf{f}}^f = \mathbf{T}^f\tilde{\mathbf{p}}^f \tag{3.17}$$

Here $\mathbf{T}^f$ is a matrix containing the fine-scale transmissibilities. The accuracy of the approximation depends on the appropriateness of the boundary conditions. In cases where flow normal to the coarse boundaries is prominent, the tangential approximation becomes questionable. Remedies are for instance investigated in [71], where a linear interpolation technique is employed to include non-local information, and in [97] where a pure algebraic method based on probing vectors is used. These approaches reduce the error in the approximation compared to the tangential approach for cases involving anisotropy and unstructured grids, but with the cost of spending more time in the construction of the basis functions.

In Paper C and D a fundamentally different approach is taken in order to assure appropriate boundary conditions for the local problems. Instead of improving the approximation to account for the anisotropy in the problem by considering more computationally involved methods, the coarse grid is adjusted to the anisotropy to make sure that a tangential approximation is appropriate. This can be seen as an analogue

to what is discussed in the gridding section for discrete fractures, where the idea is to systematically improve the quality of the grid in order to reduce the discretization error. In fractured reservoirs the dominant anisotropy is explicitly represented by the *large-scale fractures*. If the coarse dual grid is constructed such that it conforms to the *large-scale fractures* as discussed in Chapter 1.4, these fractures form natural boundary conditions for the localized problems. Moreover, the tangential approximation of excluding flow normal to the boundary is justified in cases where flow in large- scale fractures dominates. This pathway is followed and explained in detail in Paper C and D.

A coarse discretization of the equation given in (3.2) can be constructed by considering a coarse analog of the same equation, that is:

$$\int_{\partial\Omega_i^c} (\mathbf{v}\cdot\mathbf{n})\,\mathrm{dS} = \int_{\Omega_i^c} q\,\mathrm{d}\Omega \tag{3.18}$$

The only difference between equation (3.18) and (3.2) is the sup-script indicating that the integration is conducted on the coarse primal grid Ω_i^c. The integration of the right hand side is still straightforward, and focus is thus on the flux expression on the left hand side. The flux over a coarse edge j is the sum of the fine-scale fluxes over the corresponding fine-scale edges:

$$f_j^c = \sum_{k\in\mathcal{S}_j} \tilde{f}_k^f, \tag{3.19}$$

where $\mathcal{S}_j$ is the set of corresponding fine-scale edges and $\tilde{f}_k^f$ the fine-scale flux over fine-scale edge k. The support of the basis functions extends its associated primal cell, and the multiscale finite-volume method therefore yields a multi-point stencil for the coarse fluxes [49].

The coarse fluxes associated with each primal cell can further be assembled in order to express the coarse discretization found in (3.18) as a linear system:

$$\mathbf{A}^c\mathbf{p}^c = \mathbf{q}^c, \tag{3.20}$$

where $\mathbf{A}^c$ is the coarse discretization matrix, and the vector $\mathbf{q}^c$ contains the coarse right hand side.

An approximation of the fine-scale pressure solution can be reconstructed from the coarse pressure using the expression in (3.16). Fine-scale fluxes computed based on the reconstructed fine-scale pressure solution will, however, not in general be conservative. To obtain a locally conservative velocity field on the fine-scale, an additional set of basis functions, based on solving localized Neumann problems using the coarse fluxes as boundary conditions is needed [49]. Or alternatively, conservative fluxes can be obtained by a post-processing step, that involves solving similar localized problems [63]. The finite-volume formulation of the coarse equation assures that the coarse fluxes are locally conservative and thus also the solvability of the local Neumann problems.

In many cases the quality of the approximated fine-scale solution based on solving the coarse-scale equations is of poor quality. One option already discussed, is to improve the boundary conditions, still for more challenging problems, for instance involving fractures at multiple scales, a suitable coarse discretization is difficult or even impossible to construct. A more robust approach is to apply the coarse solution as a

preconditioner in an iterative setting to improve the accuracy of the fine-scale solution. The simplest such strategy is a preconditioned Richardson scheme:

$$\mathbf{p}^{k+1} = \mathbf{p}^k + \kappa \mathbf{B}_{\mathbf{MS}}(\mathbf{q} - \mathbf{A}\mathbf{p}^k), \tag{3.21}$$

where $\mathbf{B}_{\mathbf{MS}}$ represents one application of the multiscale method and κ is a damping factor. The convergence of the Richardson scheme is often slow and a better choice is a Krylov subspace based iterative solver as GMRES [94]. For a two-level method to be scalable for elliptic problems, the long-range correlations must be represented in the coarse system [101]. For fractured porous media the long-range correlation paths are explicitly given by the *large-scale fractures*. A coarse-scale model where the intersections between the *large-scale fractures* constitute the coarse variables as suggested in Paper C and D, is thus expected to be an ideal preconditioner for fractured reservoirs. Due to the special construction of the preconditioner, and the possibility of post-processing the fluxes, the iteration can be stopped whenever the desired accuracy is obtained, which is in contrast to standard preconditioners where machine accuracy must be obtained in order to assure that the resulting flux field is conservative [84]. The inexact linear solver approach is shown to be a promising approach for obtaining reasonable accurate solutions to high-resolution discrete fracture models.

3.4 Hyperbolic discretizations

This section briefly presents a finite-volume discretization of the hyperbolic equation that is applicable for the linear transport equation (2.12) considered in Paper B-D and the convective part of the temperature equation (2.14) considered in Paper A and E. Consider the following scalar hyperbolic conservation equation:

$$\frac{\partial c}{\partial t} + \nabla \cdot \boldsymbol{\theta}(c) = q^c, \tag{3.22}$$

where c is the conserved quantity, $\boldsymbol{\theta}$ is the flux function and q^c is used for the source term. In contrast to the elliptic equation, which has an infinite prorogation speed, the hyperbolic equations propagate information along characteristics with a finite speed. Explicit methods can therefore be used for the hyperbolic equations, provided they satisfy the CFL criteria [67]. In explicit methods, the shocks in the solution are preserved, but the CFL condition may constrain the size of the time-steps significantly if small cells are used.

For convergence of the numerical solution, it is sufficient for the discretization scheme to be conservative, consistent and monotone. The standard discretization for the hyperbolic equation used in most commercial simulators and also herein, is the finite-volume method with single point upstream weighting [11, 18]. The finite-volume method discretizes the conservation integral directly and is therefore conservative by construction. For simple flux functions in homogenous media, the upstream weighting is consistent, but for problems involving complex flux functions and heterogeneous media, the upstream method does not always give the relevant physical solution [76, 109]. Other discretization methods for hyperbolic conservation laws are the Gudonov method and the Enqvist-Osher method. For more details, including monotonicity conditions for hyperbolic equations, see for instance [67].

The need of efficient, yet accurate, transport solvers for high-resolution models is apparent. The research along this path can be divided into three main categories: Fast fine-scale transport solvers, for instance based on streamlines [79], higher-order methods (TVD [37], ENO [37], DG [45]) or reordering [78], multiscale transport methods [65] and flow-based coarsening/upscaling [1, 38–40]. The third option is considered in Paper D and E, and thus further discussed herein.

3.4.1 Finite-volume methods

To obtain a finite-volume formulation of the conservation equation given in (3.22), this equation is integrated in space over a finite volume Ω_i, and in time from t^n to t^{n+1},

$$\int_{\Omega_i} c^{n+1} - c^n \, \mathrm{d}\Omega = -\int_{t^n}^{t^{n+1}} \int_{\partial\Omega_i} \boldsymbol{\theta}(c) \cdot \mathbf{n} \, \mathrm{dS} \, \mathrm{dt} + \int_{t^n}^{t^{n+1}} \int_{\Omega_i} q^c \mathrm{d}\Omega \, \mathrm{dt}. \tag{3.23}$$

The divergence theorem is applied to arrive at the flux integral, and the fundamental theorem of calculus to remove the time integral in the accumulation term. Assuming the flux function $\boldsymbol{\theta}$ and the source term q^c to be constant during each time-step, the conserved quantity in cell i, c_i^{n+1} at time t^{n+1} equals the conserved quantity c_i^n at the previous step t^n, plus the influx at the boundary and the total contribution from the source term Q_i^c, or mathematically:

$$c_i^{n+1} = c_i^n - \frac{\Delta t^n}{V_i} \left(\int_{\partial\Omega_i} \boldsymbol{\theta}(c) \cdot \mathbf{n} \, \mathrm{dS} - Q_i^c \right). \tag{3.24}$$

Here V_i is the volume of the cell and the time-step $\Delta t^n = t^{n+1} - t^n$. An implicit or explicit method can be formulated from (3.24) based on whether the flux function is evaluated at the previous time step t^n or at the present t^{n+1}. For an explicit method CFL conditions restrict the size of the time stepping as discussed in the beginning of this chapter. The standard way to approximate the flux integral is to use the upstream value of the flux function [11, 67]. The upstream method is unconditionally monotone and proof of convergence for homogenous media is shown for instance in [18].

3.4.2 Flow-based upscaling

Flow-based upscaling or coarsening is applied in Paper D for the linear transport equation and in Paper E for the temperature equation in order to gain efficiency in the transport simulations. In flow-based upscaling, fine-scale information is used to construct a coarse transport model. The idea is to group cells that are believed to possess similar solution properties based on the fine-scale description. The agglomeration of the fine-scale cells can be based on flow-based indicators as localized time-of-flight calculations or the velocity field. Alternatively, error estimates, grid topology and geometry and/or expert knowledge can be used to dictate the coarsening [1, 38, 39]. A simple geometry based indicator, namely the distance to the nearest large-scale fracture, is used in Paper D and E. For fractured media this leads to coarse grids that mimics extended dual continuum or multiple interacting continuum (MINC) type models. But in contrast to the MINC type models suggested by [53, 88], where the same coarse

grid is used both for the flow and the transport equation, different levels of coarsening and solution strategies can be applied. The combination of flow-based upscaling with a multiscale method for the pressure equation as demonstrated in Paper D and E is particularly powerful as fine-scale fluxes balanced with respect to accuracy and computational cost can be used as basis for the upscaling. Moreover, as fine-scale information is available, the computation of the transfer terms between the continua is straightforward and no heuristic assumptions are needed for the interaction between the continua as in traditional dual-continuum and MINC models.

For convective transport, coarse fluxes are computed by combining associated fine-scale fluxes. The flux function can then either be evaluated prior or after the summation [39]. The first choice may lead to bi-directional flow on the coarse scale even if a single point upstream method is applied an the fine-scale. According to [38], the second option where net fluxes are used is more accurate and efficient.

If a conductive term is present in the transport equation, as in the temperature equation in (2.14), a coarse discretization of the conductive term is needed. As conduction has the same elliptic structure as the pressure equation, the multiscale methodology for the pressure equation can be used in the upscaling. With the multiscale finite-volume methodology, the coarse fluxes are conservative by construction and, moreover, a consistent multipoint approximation also of the intra block fluxes comes naturally from using basis functions in the upscaling. As this is a pure upscaling approach, there are no means to recover the fine-scale solution from the coarse solution as is possible when a multiscale method is used. But as the thermal conductivity varies much less than the permeability, the quality of the upscaled thermal conductivity is expected to be much better than for the permeability. The thermal conductivity upscaling is further discussed in Paper E.

Chapter 4

Summary of results and outlook

An approximate answer to the right question
is worth a great deal more than a precise answer to the wrong question.
John W. Tukey

In this final chapter, the main results of the work as presented in the included papers are summarized and put into a broader context. The included papers can be grouped based on their objectives. Paper A and B investigate finite-volume methods for discrete fracture-matrix models, while Paper C, D and E aim to tackle challenges related to large high-resolution models for fractured porous media.

4.1 Finite-volume methods for Discrete Fracture-Matrix models

Paper A and B present a consistent finite-volume discretization for discrete fracture-matrix models on unstructured grids with a lower-dimensional representation of the fractures. By extending the method presented by [52], which is based on a two-point flux approximation (TPFA), to a multipoint flux approximation (MPFA), consistency in the flux discretization is achieved also for general unstructured grids.

4.1.1 Summary

In Paper A, a MPFA method is successfully applied for matrix-matrix, fracture-matrix and fracture-fracture connections. In cases where more than two fracture segments meet, a so-called "start-delta" transformation is used to split the transmissibilities, similar to what is done in [52]. The new MPFA based method is compared to standard equi-dimensional discretizations and to the earlier TPFA based approach in numerical examples with promising results. The error of representing the fractures as lower-dimensional objects in the grid is small for relevant configurations, and much smaller than the error stemming from using a TPFA on an unstructured grid. The examples in this paper involve both fluid flow and heat transfer.

Paper B extends the work started in Paper A. Most importantly, a more rigorous derivation of the MPFA based method for lower-dimensional fractures is presented. Numerical examples show that splitting the transmissibilities using the "start-delta" transformation may not be consistent. A more accurate result is in fact obtained by splitting the fluxes in the transport equation, as the correct upstream values then can

be found. This paper also investigates the robustness with respect to the underlying assumptions and the efficiency of the lower-dimensional approach. Convergence analysis shows that the lower-dimensional approach is accurate for channeling fractures only in cases where the apertures are significantly smaller than the neighboring cells. It also shows that for fractures acting as barriers, this constrain on the aspect ratio can be relaxed considerably. The efficiency of the lower-dimensional approach is further shown by studying the condition number of the discretization matrix, which shows that the lower-dimensional approach is order of magnitudes better conditioned than a standard equi-dimensional approach.

4.1.2 Further directions

The MPFA framework developed for fractures can be integrated in general purpose simulators based on a finite-volume framework. In Paper A, the scheme is implemented in our in-house general purpose reservoir simulator RS [41], capable of simulating multiphase/multicomponent fluid flow. With appropriate equations of states and emphasis on the phase equilibrium calculations, multiphase flow, as well as phase changes can be modeled in combination with the proposed method. Application of MPFA methods to multiphase flow are considered in for instance [21, 62].

The inertia effects present in high-flow regimes, for instance in fractures and near injection wells, may reduce the flow velocity significantly. Such effects are observed in geothermal systems, [58, 59, 108] and are typically modeled by adding a non-linear Forchheimer correction to Darcy's equation as discussed in Chapter 2.4. Considering the Forchheimer term to be a property of the fluid, the term can be handled similar as relative permeability in finite-volume methods [8, 113]. The non-linearity is handled by iterations, for instance using a Newton algorithm with Darcy's velocity as an initial guess. Alternatively, the fracture and porous media can be formally decoupled in a domain decomposition framework such that different equations can be used on different domains [34].

4.2 Multiscale solvers and flow-based upscaling

In Paper C, D and E we aim to make an efficient simulation strategy for flow and transport in porous media that possess fractures on multiple scales. An inexact solver designed to bridge the gap between linear solvers and conventional upscaling is utilized for the pressure equation to provide a flexible approach for handling the competing demands of accuracy and computational cost that are inherently present for flow in fractured aquifers. For the transport of heat and mass, flow-based upscaling is applied in Paper D and E to speed up the calculations.

4.2.1 Summary

In Paper C different options for constructing coarse grids are compared. The result shows that for cases where fractures dominate the flow, the coarse grid should be tailored to the fracture network. That is, coarse degrees of freedom should be assigned to the intersection of fractures, and the fractures should define the coarse partitioning of

the domain. In this way, long-range correlations in the problem are represented in the coarse discretization and, moreover, the fractures form natural boundary conditions for the local sub-problems that are solved to acquire the basis functions.

In Paper D the promising results shown in Paper C are further examined. In particular, the robustness of the inexact approach with respect to *a priori* assumptions on the significance of individual fractures are demonstrated by numerical examples. In cases where the problem can be upscaled, a single iteration with little extra cost compared to standard upscaling is sufficient, while for cases where features not represented in the coarse grid becomes significant, the iterative method will efficiently resolve these. The applicability of the method to complex problems, involving deterministic as well as stochastic realizations of fractures, is further demonstrated by numerical examples. The utility of basing upscaled transport models on the approximated fine-scale fluxes is demonstrated by considering both upscaled single and dual-continuum type models.

Paper E applies the ideas presented in Paper D in a geothermal setting. The flow-based upscaling approach presented for purely convective tracer transport is extended to include conductive processes as well as convection. In particular, MINC type models based on the fine-scale description are proposed to increase the accuracy of the upscaling. The validity of the new approach, where an inexact approach is used for the pressure equation and flow-based upscaling is used for the heat transport, is shown by considering examples mimicking realistic data on multiscale fractures.

4.2.2 Further directions

The multiscale method used in these papers for the pressure equation only considers two-levels. A natural extension is thus to include more than two levels as done recently by [84]. There are two main challenges associated with extending the two-level method presented in these papers. The first challenge is the construction of the grid hierarchy for multiple levels. Adding additional complexity to the already challenging task of constructing discrete fracture grids may obstruct the multilevel approach. Still measures can be taken to ensure the quality of the grid as well as reducing the computational complexity associated with the gridding. The quality of the grid can be ensured by relaxing the accuracy of the fracture locations as discussed in Chapter 3.2. By applying different grid resolutions adapted to the spatial scales associated with the levels, the additional complexity of considering multiple levels of grids should be manageable. The computational cost can be reduced by applying the same multilevel domain decomposition strategy in the gridding. By constructing the grid recursively, level by level, and subdomain by subdomain, the gridding can be processed in parallel and, moreover, the grid hierarchy needed in the multilevel method comes automatically from the way the grid is constructed. The other challenge associated with extending the methodology to multiple level, is the post-processing of the fine-scale fluxes on arbitrary primal grids. For such grids, the local systems may be under-determined. A solution proposed by [84] is to add equations based on the first momentum of the velocity in order to obtain solvable systems.

The stop criteria used in the iterative method in these papers is either maximum number of iterations or a given tolerance of the residual. The results in Paper C and D show that the residual may not be the best indicator for the accuracy of the solution. As we are often more interested in the accuracy of the fluxes and ultimately the error

in the accumulated fluxes found in the production curves, *a posteriori* error estimates based on the post-processed fluxes as developed in [51, 84] may be a more vital option. Using these estimates the iterative solver can for instance be stopped when the error in the solver is less than the discretization error. Due to the large uncertainty in the fracture description, especially for the *small-scale fractures*, a less strict convergence criterion for the linear solver is of interest. Heuristic *a posteriori* error estimates linked to the uncertainty of the fracture description is of interest as discussed in Paper D. Similar ideas are also persuaded in [84, 92].

All examples shown in these papers are restricted to two spatial dimensions. The multiscale method itself can be generalized to N-spatial dimensions [83]. Note however that the quality of the coarse discretization may degenerate as the number of dimensions increase [96]. In three dimensions the fractures, now as planes, still form natural boundary conditions for the local problems and represent the global connections in the domain. The multiscale method is thus expected to perform well for fractured porous media also in three dimensions. Three dimensional gridding of fractures is computationally challenging. A solution is to use a domain decomposition strategy to reduce the computational cost associated with the gridding [7] as already discussed. In principle the gridding, the fine-scale discretization and the construction of the basis function can be done locally and in parallel, and thus addressing both CPU and memory challenges related to large-scale three dimensional simulations. There will however be significant computational cost associated with the partitioning and merging of the domains and this strategy is thus best suited for cases with large sub-domains. In a multilevel setting, where a less aggressive coarsening is applied at each level, such gridding strategies may be less efficient.

In Paper A and B, a lower-dimensional discretization of the fractures where developed. This new and more accurate discretization scheme is however not applied in the successive multiscale papers. The reason for this is a technical issue found when combining the multipoint upstream weighting used in the intersection of the fractures, with the post-processing algorithm of the fine-scale fluxes. As the focus in the multiscale papers is on constructing robust coarse discretizations and not on the fine-scale discretizations, solving this technical issue has not been prioritized. Moreover, as the results in Paper B show that the discrepancy between using a TPFA and a MPFA method is not severe for homogenous cases that are gridded carefully.

The flow-based transport upscaling considered in these papers uses a geometric indicator, i.e. distance to the nearest fracture, for the amalgamation of the fine cells. Other more advanced strategies based on the actual fine-scale flow field may be used as suggested in [3, 38, 39]. Basing the amalgamation on localized time-of-flight calculations improves the quality of the upscaling considerably [38], and will do the upscaling less sensitive to *a priori* assumptions on the importance of the individual fractures. If conductive fluxes are important, the amalgamation algorithm should be based on a weighting of the time-scale associated with the convective part and the conductive part as discussed in [28].

Linear transport (tracer and heat) is considered in these papers. The multiscale method has been applied for multiphase flow problems for instance in [50, 65, 70]. As suggested by these authors the basis functions should be reused adaptively for efficiency in the multiscale method. Gravity effects, capillary forces and compressibility can be included using operator splitting and additional sets of basis functions

[63, 70, 72]. For gravity or capillarity dominated problems, pressure driven flow in the *large-scale fractures* may be less prominent. A coarse operator capturing flow in the *large-scale fractures* may in such cases be less attractive. For multiphase flow the amalgamation of the cells in flow-based upscaling should be based on a weighting of the relative importance of the different processes involved. In the end, it is however important to emphasize that if there is no multiscale structure in the problem itself, using a multiscale method becomes less appealing. If fine-scale features are important as often is the case in multiphase simulations, fine-scale simulations may be inevitable.

4.3 Outlook

In the introduction, five challenges for numerical simulations of geothermal reservoirs were identified. This work has been dedicated to the fourth challenge related to high-resolution models and multiscale fractures. For the new approaches to be applicable in a geothermal setting, they must be able to include other relevant processes for simulation of geothermal reservoirs. Most notable are rock mechanics and chemistry, both phenomena closely coupled to the hydrothermal processes.

In the fracturing phase, where the reservoir is stimulated to increase its permeability, fluid is injected into the reservoir at high pressure. The fluid will flow into existing fractures and start to push the rock faces apart. The fluid pressure acts to weaken the normal stresses causing the rock to slide along faults or other planes of weaknesses. In the fracturing phase, the enhanced permeability is primarily caused by amplified apertures in existing fractures, but new fractures may also be created. In the production phase, the fluid pressure is lower and the chance of creating new fractures is less than for the stimulating phase. The changes in the fracture apertures will for both cases be small, implying that there will be no need to change the grid if a lower-dimensional modeling of the fractures is used as in Paper A and B. The proposed models are therefore suitable for coupling with a rock mechanical model for opening and closing of fractures. The exception is when new fractures are created. Then new grids must be created and an non-conforming gridding strategy as suggested in [54] may be a better option.

Chemical reactions influence the strength of the rock causing changes in the failure conditions of the rock, but more importantly precipitation may decrease the permeability and even plug pore throats and fractures, or dissolution increase the permeability by opening up pores and fractures. The chemical reactions change the volume locally, and thus influence the porosity and the permeability of the porous media and the fractures. Such chemical effects can be incorporated into finite-volume discretization of the flow equation as done for instance in [114, 115]. The dissolved chemical species are transported according to hyperbolic conservation laws suitable for finite-volume discretizations. However, the large span of time-scales for which the chemical reactions happen is a significant challenge for the numerical methods.

The main contributions of this thesis are a consistent and robust fine-scale discretization of fractures and a multiscale approach to tackle the resulting high-resolution models. Combined with recent progress on coupled THMC models, the contribution of this thesis provides improved capabilities of predicting reservoir performance in geothermal systems. Better reservoir design and production strategies can be obtained, which are important factors to increase the economic feasibility of the geothermal en-

ergy production. The author of this thesis believes that the results found in this thesis can be considered as important contributions toward making geothermal energy a major supplier of renewable energy in the world.

Bibliography

[1] AARNES, J., GIMSE, T., AND LIE, K. An introduction to the numerics of flow in porous media using MATLAB. In *Geometric Modelling, Numerical Simulation, and Optimization*, G. Hasle, K.-A. Lie, and E. Quak, Eds. Springer Berlin Heidelberg, 2007/01/01 2007, ch. 9, pp. 265–306. 3.1, 3.4, 3.4.2

[2] AARNES, J., KROGSTAD, S., AND LIE, K.-A. Multiscale mixed/mimetic methods on corner-point grids. *Comput. Geosci. 12*, 3 (2008), 297–315. 3.3

[3] AARNES, J. E., HAUGE, V. L., AND EFENDIEV, Y. Coarsening of three-dimensional structured and unstructured grids for subsurface flow. *Adv. Water Resour. 30*, 11 (2007), 2177–2193. 4.2.2

[4] AAVATSMARK, I. An introduction to the multipoint flux approximations for quadrilateral grids. *Comput. Geosci. 6*, 3-4 (2002), 405–432. 3.3, 3.3.1, 3.3.1

[5] AAVATSMARK, I., EIGESTAD, G., AND KLAUSEN, R. Numerical convergence of the MPFA O-method for general quadrilateral grids in two and three dimensions. *Ima. V. Math. 142* (2006), 1–21. 3.3.1

[6] AAVATSMARK, I., EIGESTAD, G., MALLISON, B., AND NORDBOTTEN, J. A compact multipoint flux approximation method with improved robustness. *Numer. Methods Partial Differ. Equations 24*, 5 (2008), 1329–1360. 3.3.1

[7] ADLER, P., THOVERT, J., AND MOURZENKO, V. *Fractured Porous Media*. OUP Oxford, 2012. 3.2, 4.2.2

[8] AHMADI, A., ABBASIAN ARANI, A., AND LASSEUX, D. Numerical simulation of two-phase inertial flow in heterogeneous porous media. *Transp. Porous Med. 84*, 1 (2010/08/01 2010), 177–200. 4.1.2

[9] ALBOIN, C., JAFFRÉ, J., AND SERRES, C. Modeling fractures as interfaces for flow and transport in porous media. In *Proceedings of an AMS-IMS-SIAM Joint Summer Research Conference on Fluid Flow and Transport in Porous Media, Mathematical and Numerical Treatment, June 17-21, 2001, Mount Holyoke College, South Hadley, Massachusetts* (2002), vol. 295, Amer Mathematical Society, p. 13. 3.3

[10] ARVIZU, D., BRUCKNER, T., CHUM, H., EDENHOFER, O., ESTEFEN, S., FAAIJ, A., FISCHEDICK, M., HANSEN, G., HIRIART, G., HOHMEYER, O., HOLLANDS, K. G. T., HUCKERBY, J., KADNER, S., KILLINGTVEIT, A., KUMAR, A., LEWIS, A., LUCON, O., MATSCHOSS, P., MAURICE, L., MIRZA,

M., MITCHELL, C., MOOMAW, W., MOREIRA, J., NILSSON, L. J., NYBOER, J., PICHS-MADRUGA, R., SATHAYE, J., SAWIN, J. L., SCHAEFFER, R., SCHEI, T. A., SCHLÄMER, S., SEYBOTH, K., SIMS, R., SINDEN, G., SOKONA, Y., STECHOW, C. V., STECKEL, J., VERBRUGGEN, A., WISER, R., YAMBA, F., AND ZWICKEL, T. Technical summary. In *IPCC Special Report on Renewable Energy Sources and Climate Change Mitigation*, O. Edenhofer, R. Pichs-Madruga, Y. Sokona, K. Seyboth, P. Matschoss, S. Kadner, T. Zwickel, P. Eickemeier, G. Hansen, S. Schlämer, and C. von Stechow, Eds. Cambridge University Press, Cambridge, United Kingdom and New York, NY, USA, 2011. (document)

[11] AZIZ, K., AND SETTARI, A. *Petroleum Reservoir Simulation*. Chapman & Hall, 1979. ISBN: 0-85334-787-5. 3.1, 3.3.1, 3.4, 3.4.1

[12] BARENBLATT, G. E., ZHELTOV, I., AND KOCHINA, I. Basic concepts in the theory of seepage of homogeneous liquids in fissured rocks. *J.Appl.Math, USSR 24*, 5 (1960), 1286–1303. 1.3

[13] BASTIAN, P., CHEN, Z., EWING, R., HELMIG, R., JAKOBS, H., AND REICHENBERGER, V. Numerical simulation of multiphase flow in fractured porous media. In *Numerical Treatment of Multiphase Flows in Porous Media*, Z. Chen, R. Ewing, and Z.-C. Shi, Eds., vol. 552 of *Lecture Notes in Physics*. Springer Berlin Heidelberg, 2000/01/01 2000, ch. 4, pp. 50–68. 3.3

[14] BEAR, J. *Dynamics of Fluids in Porous Media*. Dover Publications, 1988. 2, 2.1, 2.1.1, 2.1.2

[15] BENZI, M. Preconditioning techniques for large linear systems: A survey. *J. Comput. Phys. 182*, 2 (2002), 418–477. 3.1

[16] BERKOWITZ, B. Characterizing flow and transport in fractured geological media: A review. *Adv. Water Resour. 25*, 8-12 (2002), 861–884. 1.3, 2.1.3

[17] BODVARSSON, G., PRUESS, K., AND LIPPMANN, M. Modeling of geothermal systems. *J. Petrol. Technol. 38*, 9 (1986), 1007–1021. (document)

[18] BRENIER, Y., AND JAFFRÉ, J. Upstream differencing for multiphase flow in reservoir simulation. *SIAM J. Numer. Anal. 28*, 3 (1991), 685–696. 3.4, 3.4.1

[19] BREZZI, F., LIPNIKOV, K., AND SIMONCINI, V. A family of mimetic finite difference methods on polygonal and polyhedral meshes. *Math. Mod. Meth. Appl. Sci. 15*, 10 (2005), 1533–1551. 3.3

[20] CACAS, M., LEDOUX, E., DE MARSILY, G., BARBREAU, A., CALMELS, P., GAILLARD, B., AND MARGRITTA, R. Modeling fracture flow with a stochastic discrete fracture network: Calibration and validation: 2. The transport model. *Water Resour. Res. 26*, 3 (1990), 491–500. 1.3

[21] CAO, H. *Development of techniques for general purpose simulators*. PhD thesis, Stanford University, 2002. 4.1.2

[22] CARLO, D., AND SCOTTI, A. A mixed finite element method for Darcy flow in fractured porous media with non-matching grids. *ESAIM-Math. Model. Num. 46*, 02 (2012), 465–489. 3.2, 3.3

[23] CHAVENT, G., AND JAFFRÉ, J. *Mathematical Models and Finite Elements for Reservoir Simulation: Single Phase, Multiphase, and Multicomponent Flows Through Porous Media*. North-Holland, 1986. 2, 3.3

[24] CHEN, Z., AND HOU, T. A mixed multiscale finite element method for elliptic problems with oscillating coefficients. *Math. Comput. 72*, 242 (2003), 541–576. 3.3

[25] CHEN, Z., HUAN, G., AND MA, Y. *Computational Methods for Multiphase Flows in Porous Media*. Society for Industrial and Applied Mathematics, 2006. 2, 2.6.1, 2.6.1, 3.1, 3.3

[26] DANKO, G., AND BAHRAMI, D. Coupled multiflux TOUGH2-TOUGHREACT THMC model for EGS studies. In *TOUGH Symposium Lawrence Berkeley National Laboratory, Berkeley, California, September 17-19* (2012). (document)

[27] DERSHOWITZ, B., LAPOINTE, P., EIBEN, T., AND WEI, L. Integration of discrete feature network methods with conventional simulator approaches. *SPE Reserv. Eval. Eng. 3*, 2 (2000), 165–170. 1.3

[28] DIETRICH, P., HELMIG, R., SAUTER, M., HÖTZL, H., KÖNGETER, J., AND TEUTSCH, G. *Flow and transport in fractured porous media*. Springer, 2005. 1.3, 2.1.3, 2.1.3, 4.2.2

[29] EDWARDS, M. G., AND ROGERS, C. F. Finite volume discretization with imposed flux continuity for the general tensor pressure equation. *Comput. Geosci. 2*, 4 (1998), 259–290. 3.3, 3.3.1

[30] EFENDIEV, Y., AND HOU, T. *Multiscale finite element methods: Theory and applications*. Springer, 2009. 3.3

[31] EVANS, L. *Partial Differential Equations*. American Mathematical Society, 2010. 3.3

[32] FAIRLEY, J., INGEBRITSEN, S., AND PODGORNEY, R. Challenges for numerical modeling of enhanced geothermal systems. *Ground water 48*, 4 (2010), 482. (document)

[33] FAKCHAROENPHOL, P., AND WU, Y. A coupled flow-geomechanics model for fluid and heat flow for enhanced geothermal reservoirs. In *45th US Rock Mechanics/Geomechanics Symposium* (2011). (document)

[34] FRIH, N., ROBERTS, J., AND SAADA, A. Modeling fractures as interfaces: a model for Forchheimer fractures. *Comput. Geosci. 12*, 1 (2008/03/01 2008), 91–104. 4.1.2

[35] FRIIS, H., EDWARDS, M., AND MYKKELTVEIT, J. Symmetric positive definite flux-continuous full-tensor finite-volume schemes on unstructured cell-centered triangular grids. *SIAM J. Sci. Comput. 31*, 2 (2008), 1192–1220. 3.3.1

[36] GOLDSTEIN, B., HIRIART, G., BERTANI, R., BROMLEY, C., GUTIÃRREZ-NEGRÃN, L., HUENGES, E., MURAOKA, H., RAGNARSSON, A., TESTER, J., AND ZUI, V. Geothermal energy. In *IPCC Special Report on Renewable Energy Sources and Climate Change Mitigation*, O. Edenhofer, R. Pichs-Madruga, Y. Sokona, K. Seyboth, P. Matschoss, S. Kadner, T. Zwickel, P. Eickemeier, G. Hansen, S. Schlömer, and C. von Stechow, Eds. Cambridge University Press, Cambridge, United Kingdom and New York, NY, USA, 2011. (document), 1.2

[37] HARTEN, A. High resolution schemes for hyperbolic conservation laws. *J. Comput. Phys. 49*, 3 (1983), 357–393. 3.4

[38] HAUGE, V., LIE, K., AND NATVIG, J. Flow-based coarsening for multiscale simulation of transport in porous media. *Comput. Geosci. 16*, 2 (2012), 391–408. 3.4, 3.4.2, 4.2.2

[39] HAUGE, V. L., AND AARNES, J. Modeling of two-phase flow in fractured porous media on unstructured non-uniformly coarsened grids. *Transp. Porous Med. 77*, 3 (2009/04/01 2009), 373–398. 1.3, 3.4, 3.4.2, 4.2.2

[40] HE, C., AND DURLOFSKY, L. J. Structured flow-based gridding and upscaling for modeling subsurface flow. *Adv. Water Resour. 29*, 12 (2006), 1876–1892. 3.4

[41] HEIMSUND, B. *Mathematical and numerical methods for reservoir fluid flow simulation*. PhD thesis, University of Bergen, 2005. 4.1.2

[42] HESTENES, M., AND STIEFEL, E. Methods of conjugate gradients for solving linear systems. *J. Res. Nat. Bur. Stand. 49*, 6 (1952), 409–436. 3.1

[43] HOLM, R., KAUFMANN, R., HEIMSUND, B., ØIAN, E., AND ESPEDAL, M. Meshing of domains with complex internal geometries. *Numer. Linear Algerbr. 13*, 9 (2006), 717–731. 1.2, 3.2, 3.1

[44] HOTEIT, H., AND FIROOZABADI, A. Multicomponent fluid flow by discontinuous Galerkin and mixed methods in unfractured and fractured media. *Water Resour. Res. 41*, 11 (2005), W11412. 3.2

[45] HOTEIT, H., AND FIROOZABADI, A. An efficient numerical model for incompressible two-phase flow in fractured media. *Adv. Water Resour. 31*, 6 (2008), 891–905. 3.4

[46] HOU, T., AND WU, X.-H. A multiscale finite element method for elliptic problems in composite materials and porous media. *J. Comput. Phys. 134*, 1 (1997), 169–189. 3.3, 3.3.3

[47] HUI, M.-H., MALLISON, B., AND LIM, K.-T. An innovative workflow to model fractures in a giant carbonate reservoir. In *International Petroleum Technology Conference, Kuala Lumpur, Malaysia, 3-5 December* (2008). 1.3

[48] INTERNATIONAL ENERGY AGENCY. Key world energy statistics from the IEA, 2011. (document)

[49] JENNY, P., LEE, S., AND TCHELEPI, H. Multi-scale finite-volume method for elliptic problems in subsurface flow simulation. *J. Comput. Phys. 187*, 1 (2003), 47–67. 1.4, 3.3, 3.3.3, 3.3.3, 3.3.3

[50] JENNY, P., LEE, S., AND TCHELEPI, H. Adaptive multiscale finite-volume method for multiphase flow and transport in porous media. *Multiscale Model. Simul. 3*, 1 (2005), 50–64. 4.2.2

[51] JIRÁNEK, P., STRAKOŠ, Z., AND VOHRALÍK, M. A posteriori error estimates including algebraic error and stopping criteria for iterative solvers. *SIAM J. Sci. Comput. 32*, 3 (2010), 1567–1590. 4.2.2

[52] KARIMI-FARD, M., DURLOFSKY, L., AND AZIZ, K. An efficient discrete-fracture model applicable for general-purpose reservoir simulators. *SPE J 9*, 2 (2004), 227–236. 3.3, 3.3.2, 4.1, 4.1.1

[53] KARIMI-FARD, M., GONG, B., AND DURLOFSKY, L. K. Generation of coarse-scale continuum flow models from detailed fracture characterizations. *Water Resour. Res. 42* (2006), W10423. 1.3, 3.4.2

[54] KARVOUNIS, D., AND JENNY, P. Modeling of flow and transport in enhanced geothermal systems. In *Thirty-Sixth Workshop on Geothermal Reservoir Engineering, Stanford University, California* (2011). (document), 4.3

[55] KAVIANY, M. *Principles of Heat Transfer in Porous Media*. Springer, 1995. 1.2, 2, 2.3, 2.6, 2.6.1, 2.6.2

[56] KLAUSEN, R., RADU, F., AND EIGESTAD, G. Convergence of MPFA on triangulations and for Richards' equation. *Int. J. Numer. Methods Fluids 58*, 12 (2008), 1327–1351. 3.3.1

[57] KLAUSEN, R. A., AND WINTHER, R. Convergence of multipoint flux approximations on quadrilateral grids. *Numer. Methods Partial Differ. Equations 22*, 6 (2006), 1438–1454. 3.3.1

[58] KOHL, T., EVANS, K., HOPKIRK, J., JUNG, R., AND RYBACH, L. Observation and simulation of non-Darcian flow transients in fractured rock. *Water Resour. Res. 33*, 3 (1997), 407–418. 4.1.2

[59] KOLDITZ, O. Non-linear flow in fractured rock. *Int. J. Numer. Method. H. 11*, 6 (2001), 547–575. 4.1.2

[60] KOSACK, C., VOGT, C., RATH, V., AND MARQUART, G. Stochastic estimates of the permeability field of the Soultz-sous-Forêts geothermal reservoir-comparison of bayesian inversion, MC geostatistics, and EnKF assimilation. In *EGU General Assembly Conference Abstracts* (2010), vol. 12, p. 4383. 2.1.2

[61] LAIDLER, K., MEISER, J., AND SANCTUARY, B. *Physical Chemistry*. Houghton Mifflin, 2002. 2.2.3

[62] LEE, S., JENNY, P., AND TCHELEPI, H. A finite-volume method with hexahedral multiblock grids for modeling flow in porous media. *Comput. Geosci. 6*, 3 (2002), 353–379. 4.1.2

[63] LEE, S., WOLFSTEINER, C., AND TCHELEPI, H. Multiscale finite-volume formulation for multiphase flow in porous media: Black oil formulation of compressible, three-phase flow with gravity. *Comput. Geosci. 12*, 3 (2008), 351–366. 3.3.3, 4.2.2

[64] LEE, S. H., LOUGH, M. F., AND JENSEN, C. L. Hierarchical modeling of flow in naturally fractured formations with multiple length scales. *Water Resour. Res. 37*, 3 (2001), 443–455. 1.3, 3.2

[65] LEE, S. H., ZHOU, H., AND TCHELEPI, H. A. Adaptive multiscale finite-volume method for nonlinear multiphase transport in heterogeneous formations. *J. Comput. Phys. 228*, 24 (2009), 9036–9058. 3.4, 4.2.2

[66] LEVEQUE, R. *Numerical Methods for Conservation Laws*. Birkhäuser, 1992. 3.3

[67] LEVEQUE, R. *Finite Volume Methods for Hyperbolic Problems*. Cambridge University Press, 2002. 3.1, 3.4, 3.4.1

[68] LIE, K., KROGSTAD, S., LIGAARDEN, I., NATVIG, J., NILSEN, H., AND SKAFLESTAD, B. Open-source MATLAB implementation of consistent discretisations on complex grids. *Comput. Geosci. 16*, 2 (2012), 297–322. 3.3

[69] LONG, J., REMER, J., WILSON, C., AND WITHERSPOON, P. Porous media equivalents for networks of discontinuous fractures. *Water Resour. Res. 18*, 3 (1982), 645–658. 1.3

[70] LUNATI, I., AND JENNY, P. Multiscale finite-volume method for compressible multiphase flow in porous media. *J. Comput. Phys. 216*, 2 (2006), 616–636. 4.2.2

[71] LUNATI, I., AND JENNY, P. Treating highly anisotropic subsurface flow with the multiscale finite-volume method. *SIAM Multiscale Model. Simul. 6*, 1 (2007), 308–318. 3.3.3

[72] LUNATI, I., AND JENNY, P. Multiscale finite-volume method for density-driven flow in porous media. *Comput. Geosci. 12*, 3 (2008/09/01 2008), 337–350. 4.2.2

[73] MALLISON, B. T., HUI, M., AND NARR, W. Practical gridding algrorithms for descrete-fracture modeling workflows. In *ECMOR XII 6-9* (Oxford, UK, 2010). 3.2

[74] MARTIN, V., JAFFRÉ, J., AND ROBERTS, J. Modeling fractures and barriers as interfaces for flow in porous media. *SIAM J. Sci. Comput. 26*, 5 (2005), 1667–1691. 3.3

[75] MATTHAI, S., MEZENTSEV, A., AND BELAYNEH, M. Finite element-node-centered finite-volume two-phase-flow experiments with fractured rock represented by unstructured hybrid-element meshes. *SPE Reserv. Eval. Eng. 10*, 6 (2007), 740–756. 3.3

[76] MISHRA, S., AND JAFFRÉ, J. On the upstream mobility scheme for two-phase flow in porous media. *Comput. Geosci. 14* (2010), 105–124, doi: 10.1007/s10596-009-9135-0. 3.4

[77] MUSTAPHA, H., DIMITRAKOPOULOS, R., GRAF, T., AND FIROOZABADI, A. An efficient method for discretizing 3D fractured media for subsurface flow and transport simulations. *Int. J. Numer. Methods Fluids 67*, 5 (2010), 651–670. 3.2

[78] NATVIG, J., AND LIE, K. Fast computation of multiphase flow in porous media by implicit discontinuous Galerkin schemes with optimal ordering of elements. *J. Comput. Phys. 227*, 24 (2008), 10108–10124. 3.4

[79] NATVIG, J., SKAFLESTAD, B., BRATVEDT, F., BRATVEDT, K., LIE, K., LAPTEV, V., AND KHATANIAR, S. Multiscale mimetic solvers for efficient streamline simulation of fractured reservoirs. *SPE J 16*, 4 (2011), 880–888. 3.3, 3.4

[80] NELSON, R. Fractured reservoirs: turning knowledge into practice. *J. Petrol. Technol. 39*, 4 (1987), 407–414. (document)

[81] NORDBOTTEN, J., AAVATSMARK, I., AND EIGESTAD, G. Monotonicity of control volume methods. *Numer. Math. 106*, 2 (2007), 255–288. 3.3.1, 3.3.1

[82] NORDBOTTEN, J., AND CELIA, M. *Geological Storage of CO2: Modeling Approaches for Large-Scale Simulation*. Wiley, 2011. 1.4

[83] NORDBOTTEN, J., KEILEGAVLEN, E., AND SANDVIN, A. Mass conservative domain decomposition for porous media flow. Tech. rep., Finite Volume Method - Powerful Means of Engineering Design, PhD. Radostina Petrova (Ed.), ISBN: 978-953-51-0445-2, InTech., 2012. 3.3.3, 4.2.2

[84] NORDBOTTEN, J. M., AND KEILEGAVLEN, E. Inexact linear solvers for multi-level control volume discretizations. *Submitted to SIAM J. Sci. Comp.* (2012). 3.3.3, 4.2.2

[85] OUENES, A., AND HARTLEY, L. Integrated fractured reservoir modeling using both discrete and continuum approaches. In *SPE Annual Technical Conference and Exhibition, Dallas, Texas,1-4 October* (2000). Paper Number 62939-MS. 1.3

[86] PODGORNEY, R., LU, C., AND HUANG, H. Thermo-hydro-mechanical modeling of working fluid injection and thermal energy extraction in EGS fractures and rock matrix. Tech. rep., Idaho National Laboratory (INL), 2012. (document)

[87] PRUESS, K. The TOUGH codes - A family of simulation tools for multiphase flow and transport processes in permeable media. *Vadose Zone J. 3*, 3 (2004), 738–746. 2.6.1, 3.1, 3.3

[88] PRUESS, K., AND NARASIMHAN, T. A practical method for modeling fluid and heat flow in fractured porous media. *SPE J 25*, 1 (1985), 14–26. Lawrence Berkeley Laboratory. 1.3, 3.4.2

[89] RADILLA, G., SAUSSE, J., SANJUAN, B., AND FOURAR, M. Interpreting tracer tests in the enhanced geothermal system (EGS) of Soultz-sous-Foréts using the equivalent stratified medium approach. *Geothermics 44*, 0 (2012), 43–51. 1.2

[90] REICHENBERGER, V., JAKOBS, H., BASTIAN, P., AND HELMIG, R. A mixed-dimensional finite volume method for two-phase flow in fractured porous media. *Adv. Water Resour. 29*, 7 (2006), 1020–1036. 3.3

[91] REICHENBERGER, V., JAKOBS, H., BASTIAN, P., HELMIG, R., AND NIESSNER, J. Complex gas-water processess in discrete fracture-matrix systems. Upscaling, mass-conservative discretization and efficient multilevel solution. Tech. rep., Technisher Bericht Heft 130, IWS ISBN: 3-9337 61-22-6, 2004. 3.2, 3.2

[92] REPIN, S. *A posteriori estimates for partial differential equations*, vol. 4. de Gruyter, 2008. 4.2.2

[93] RYBACH, L., AND MONGILLO, M. Geothermal sustainability - a review with identified research needs. *GRC Transactions 30* (2006), 1083–1090. (document)

[94] SAAD, Y., AND SCHULTZ, M. GMRES: A generalized minimal residual algorithm for solving nonsymmetric linear systems. *SIAM J. Sci. Stat. Comput. 7*, 3 (1986), 856–869. 3.1, 3.3.3

[95] SAHIMI, M. *Flow and Transport in Porous Media and Fractured Rock*. John Wiley & Sons, 2011. 1.3

[96] SANDVIN, A., KEILEGAVLEN, E., AND NORDBOTTEN, J. Auxiliary variables in multiscale simulations. *Submitted to J. Comput. Phys.* (2012). 4.2.2

[97] SANDVIN, A., NORDBOTTEN, J., AND AAVATSMARK, I. Multiscale mass conservative domain decomposition preconditioners for elliptic problems on irregular grids. *Comput. Geosci. 15*, 3 (2011), 587–602. 3.3.3

[98] SCHLUMBERGER. Eclipse technical description, s.l.: s.n,, 2010. 3.3

[99] SHEWCHUK, J. R. Triangle: Engineering a 2D Quality Mesh Generator and Delaunay Triangulator. In *Applied Computational Geometry: Towards Geometric Engineering*, M. C. Lin and D. Manocha, Eds., vol. 1148. Springer-Verlag, 1996, pp. 203–222. From the First ACM Workshop on Applied Computational Geometry. 3.2

[100] SLEIJPEN, G., AND FOKKEMA, D. BiCGstab (l) for linear equations involving unsymmetric matrices with complex spectrum. *Electron. Trans. Numer. Anal. 1*, 11 (1993), 2000. 3.1

[101] SMITH, B., BJØRSTAD, P., AND GROPP, W. *Domain Decomposition: Parallel Multilevel Methods for Elliptic Partial Differential Equations*. Cambridge University Press, 2004. 3.1, 3.3.3

[102] SURMA, F., AND GERAUD, Y. Porosity and thermal conductivity of the Soultz-sous-Forêts granite. *Pure Appl. Geophys. 160*, 5-6 (2003/05/01 2003), 1125–1136. 2.1.1

[103] TARON, J., AND ELSWORTH, D. Thermal-hydrologic-mechanical-chemical processes in the evolution of engineered geothermal reservoirs. *Int. J. Rock Mech. Min. Sci. 46*, 5 (2009), 855–864. (document)

[104] TARON, J., AND ELSWORTH, D. Coupled mechanical and chemical processes in engineered geothermal reservoirs with dynamic permeability. *Int. J. Rock Mech. Min. Sci. 47*, 8 (2010), 1339–1348. (document)

[105] TARON, J., ELSWORTH, D., AND MIN, K.-B. Numerical simulation of thermal-hydrologic-mechanical-chemical processes in deformable, fractured porous media. *Int. J. Rock Mech. Min. Sci. 46*, 5 (2009), 842–854. (document)

[106] THOMAS, G., AND THURNAU, D. Reservoir simulation using an adaptive implicit method. *Old SPE Journal 23*, 5 (1983), 759–768. 3.1

[107] TOSELLI, A., AND WIDLUND, O. *Domain Decomposition Methods - Algorithms and Theory*. Springer, 2005. 3.1

[108] TULINIUS, H., AXELSSON, G., TOMASSON, J., KRISTMANNSDOTTIR, H., AND GUDMUNDSSON, A. Stimulation of well SN-12 in the Seltjarnarnes low-temperature field in SW-Iceland. In *Proceedings of the 21st Workshop on Geothermal Reservoir Engineering* (1996), pp. 489–496. 4.1.2

[109] TVEIT, S., AND AAVATSMARK, I. Errors in the upstream mobility scheme for countercurrent two-phase flow in heterogeneous porous media. *Comput. Geosci. 16*, 3 (2012/06/01 2012), 809–825. 3.4

[110] WANG, W., KOSAKOWSKI, G., AND KOLDITZ, O. A parallel finite element scheme for thermo-hydro-mechanical (THM) coupled problems in porous media. *Comput. Geosci. 35*, 8 (2009), 1631–1641. (document)

[111] WELTY, J., WICKS, C., AND WILSON, R. *Fundamentals of momentum, heat, and mass transfer*. J. Wiley, 1969. 2.6.1

[112] WHITAKER, S. Advances in theory of fluid motion in porous media. *Ind. Eng. Chem. 61*, 12 (1969), 14–28, doi: 10.1021/ie50720a004. 2.4, 2.4

[113] WU, Y.-S. Numerical simulation of single-phase and multiphase non-Darcy flow in porous and fractured reservoirs. *Transp. Porous Med. 49*, 2 (2002/11/01 2002), 209–240. 4.1.2

[114] XU, T., AND PRUESS, K. Modeling multiphase non-isothermal fluid flow and reactive geochemical transport in variably saturated fractured rocks: 1. Methodology. *Am. J. Sci. 301*, 1 (2001), 16–33. (document), 4.3

[115] XU, T., SONNENTHAL, E., SPYCHER, N., AND PRUESS, K. TOUGHREACT-A simulation program for non-isothermal multiphase reactive geochemical transport in variably saturated geologic media: Applications to geothermal injectivity and CO2 geological sequestration. *Comput. Geosci. 32*, 2 (2006), 145–165. (document), 4.3

[116] YANG, J., SAN, W., ZOU, H., AND LIANG, G. A new mesh generation strategy and related algorithm for discrete fracture model in naturally fractured reservoir numerical simulation. In *Recent Advances in Computer Science and Information Engineering*, Z. Qian, L. Cao, W. Su, T. Wang, and H. Yang, Eds., vol. 126 of *Lecture Notes in Electrical Engineering*. Springer Berlin Heidelberg, 2012/01/01 2012, ch. 9, pp. 63–69. 3.2